6-1-2018

Unbiased spontaneous solar fuel production using stable composite nanofiber photocatalysts

Menna Hasan

Recommended Citation

APA Citation

Hasan, M. (2018).*Unbiased spontaneous solar fuel production using stable composite nanofiber photocatalysts* [Master's Thesis, the American University in Cairo]. AUC Knowledge Fountain.
https://fount.aucegypt.edu/etds/451

MLA Citation

Hasan, Menna. *Unbiased spontaneous solar fuel production using stable composite nanofiber photocatalysts*. 2018. American University in Cairo, Master's Thesis. *AUC Knowledge Fountain*.
https://fount.aucegypt.edu/etds/451

The American University in Cairo

The Graduate School

The Nanotechnology Program

Unbiased Spontaneous Solar Fuel Production Using Stable Composite Nanofiber Photocatalysts

A Thesis in

Nanotechnology

By

Menna Mohamed Hasan

Submitted in Partial Fulfillment

of the Requirements for the Degree of

Masters of Science in Nanotechnology

May 2018

The thesis of Your Name was reviewed and approved* by the following:

Nageh K. Allam
Associate Professor and Graduate Director
Physics Department, The American University in Cairo
Thesis Advisor
Chair of Committee

Salah M. El-Sheikh
Professor of Physics
The American University in Cairo
Internal Examiner

Eman El-Mahallawi
Professor of Materials Science and Engineering
Cairo University
External Examiner

Adel Awad
Professor of Physics
The American University in Cairo
Moderator

*Signatures are on file in the Graduate School

ABSTRACT

It is becoming more urgent every day to find an efficient alternative to fossil fuels. This need motivates the search for a low-cost and stable photocatalysts to split water and generate hydrogen gas as a clean and renewable source of energy. In this thesis, novel TiO_2-CuO and TiO_2-Cu composite nanofibers were fabricated and tested for solar hydrogen generation. The effect of annealing the nanofibers in different atmospheres on their crystal structure and morphology was investigated and correlated to the photocatalytic activity of the materials using XRD, electron paramagnetic resonance (EPR) techniques, transmission electron microscopy TEM, and Fourier transform infrared FTIR. The optical properties of the fabricated nanofibers were investigated using UV-Vis spectroscopy. The absorption spectra showed that the addition of both CuO or Cu to TiO_2 shifts the absorption edge into the visible region of the solar spectrum. The photocatalytic activity and stability of the fabricated nanofibers were tested in a UV-reactor. The metallic copper supported TiO_2 nanofibers showed significant enhancement in the amount of hydrogen evolved during the photocatalytic water splitting process. This enhancement can be related to the distinct characteristics of the material including, high surface area and increasing the life time of the photogenerated charge carriers that results in efficient charge separation. The fabricated TiO_2-CuO composite nanofibers showed 117% enhancement in the amount of hydrogen evolved during the photocatalytic water splitting process compared to TiO_2 nanofibers. On the other hand, TiO_2-Cu composite nanofibers showed 344% enhancement compared to that of TiO_2 nanofibers. The study showed that Cu is a promising alternative to noble metals as a catalyst in photocatalytic water splitting, with the advantage of being an earth abundant element and a relatively cheap material.

TABLE OF CONTENTS

LIST OF FIGURES

LIST OF TABLES

ACKNOWLEDGEMENTS

I thank Allah subhanahu wa ta’ala for all the blessings that he gave me. I thank Allah for the blessing of having a loving family. I really appreciate their support, especially my mother and my father. I could not have done it without their care and guidance, and I ask Allah subhanahu wa ta’ala to reward them in this life and the afterlife. I also thank Allah for having a loving sister and brothers, who have been always the source of joy in my life, and for being always there for me.

I would also like to thank Dr. Nageh Allam not just for being my advisor, but also for being a mentor through the tough times. For expanding my limits and helping me discover new potentials in myself that I did not even know that I have.

I am also very grateful to all EML group members, who have shown me the real meaning of being brothers and sisters in Islam and taught me how to be kind, and many other beautiful and precious meanings. I owe each one of them, and I wish that someday I can pay them back.

I also have the deepest gratitude to my school, and to my teachers and all the professors who taught me.

At the end I would like to thank AlGhurair Foundation for funding my master’s studies.

DEDICATION

I dedicate this thesis to my brother Omar Sardina. May he rest in peace and may Allah accept him in paradise.

Chapter 1

Introduction and Scope of the Thesis

1.1 The Energy Demand

1.1.1 Energy Demand and Environment Global Considerations

The increasing demand on energy and the need for a solution for the global warming problem are two major challenges that are being studied globally. The International Energy Agency (IGA) published the World Energy Outlook 2011, in which they expect the global energy demand to increase dramatically by 40 % from 2009 to 2035. Today, the world mainly depends on fossil fuels as the primary sources of energy to satisfy the energy demands of the globe, Figure 1.1.b. However, these resources are nonrenewable and have negative impacts on the environment.[1–3] Combustion of fossil fuels results in air pollutants, such as, heavy metals and sulfur oxides, as well as increasing the concentration of CO_2 in the atmosphere, as shown in Figure 1.1a. CO_2 is a greenhouse gas and one of the main causes of the global warming phenomena.[4–6]

1.1.2 Renewable and Clean Sources of Energy

As mentioned in the previous section, the world is depending mainly on fossil fuels to get the energy needed for human beings to sustain. However, human population is increasing rapidly and more fossil fuels are being consumed, resulting in more polluting emissions. Therefore, the need for sustainable and clean sources of energy became an urgent need. Different Renewable energy sources have been introduced during the past few decades, such as wind power, hydro power, solar energy, bioenergy, and geothermal energy.[7] In this thesis, our interest is mainly about solar energy-driven hydrogen production. Hydrogen gas is an energy source that can provide almost three times the energy provided by gasoline for instance, with the advantage of being a sustainable and clean source of energy that when combusted does not release any polluting gases.[8]

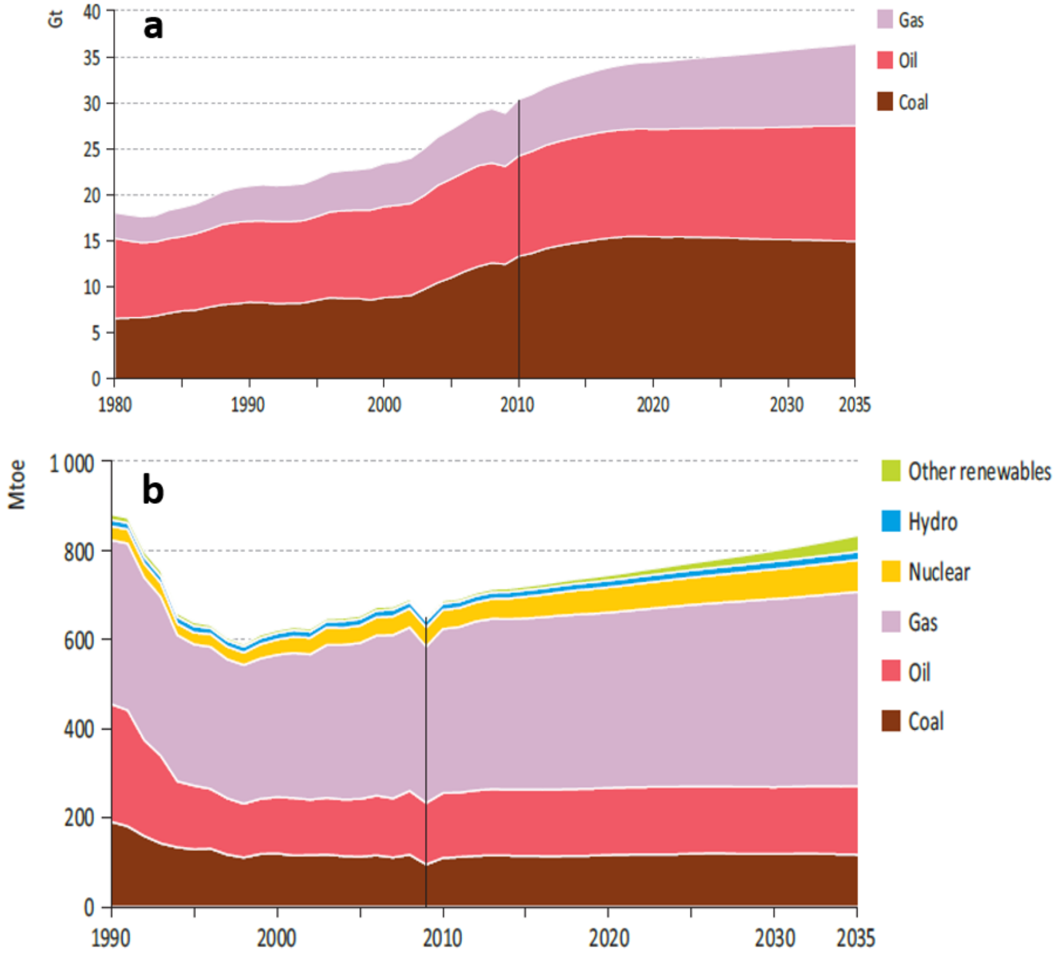

Figure 1.1. (a) Energy-related CO_2 emissions. (b) World primary energy demand of fuel.[2]

1.1.3 Energy Driven Water Splitting

According to thermodynamics, water splitting is a nonspontaneous reaction. This means that energy must be introduced to the system to drive the reaction. As shown in Figure 1.2, different forms of energy can be used to provide the system with the energy needed, such as, electrical, thermochemical, biochemical, photonic energy, or hybrid of two types or more.[7] This thesis mainly targets utilizing photonic energy to perform photocatalytic water splitting.

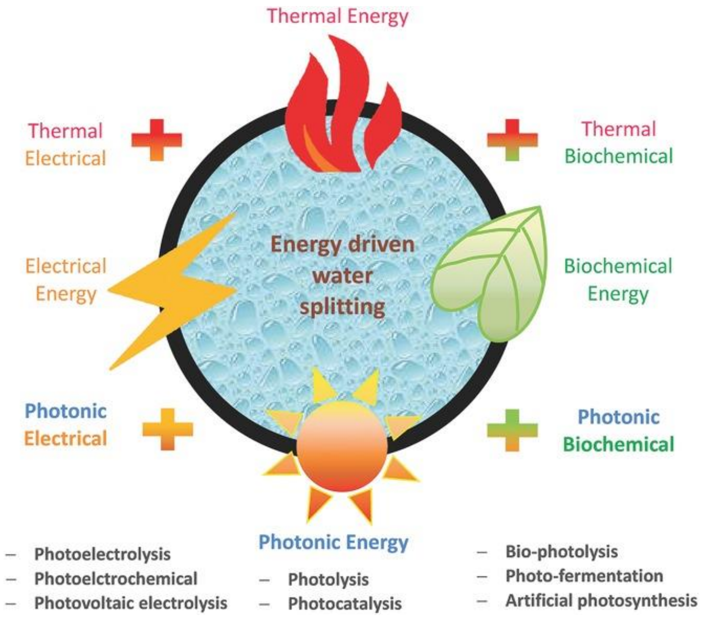

Figure 1.2 Different water splitting techniques using photonic, electrical, thermal, and biochemical energy or hybrid systems.[7]

1.2 Photocatalysts

1.2.1 Design and Description

An efficient photocatalyst for photocatalytic water splitting should have a band gap of at least 1.23 eV and be stable against photocorrosion. Moreover, small size and high crystallinity are favorable to enhance charge separation and minimize the losses due to charge recombination. So far, various groups of materials have been tested as catalysts for water splitting such as, metal oxides, nitrides, sulfides, perovskites, lanthanides and phosphates with d^{10} and d^0 electronic configuration, etc.[9]

1.2.2 Restrictions of the Photocatalyst Material

Figure 1.3 summarizes the band structure of different semiconductors and their positions with respect to the redox potentials of water, and the limitations related to each one of them. The first problem is having a large band gap that reduces the absorption to a very small part of the solar spectrum, and accordingly the electrons in the valence band requires high energy to be excited to the conduction band. Another issue arises if the catalyst's band edge position is not suitable for the electrons in the conduction band and holes in the valence band of the semiconductor to be transferred to the water molecules to perform the targeted redox reaction. Finally, some of the catalysts explored are not stable, thus they are easily corroded after a very short time.[10]

1.2.3 Suggested Solutions

The problems mentioned in the previous section can be overcome by doping these photocatalysts by ions such as $V^{5+,}$ $Ni^{2+,}$ and Cr^{3+}. These transition metal cations can narrow the band gap of the semiconductor and extend its absorption towards the visible region of the solar spectrum. Co-catalysts such as Pt, NiO, Au, and RuO_2 can be used to overcome charge recombination and facilitate the charge transfer process due to the electric field formed because of the heterojunction at the metal/semiconductor interface, this can greatly enhance the efficiency of the overall water splitting process.[9]

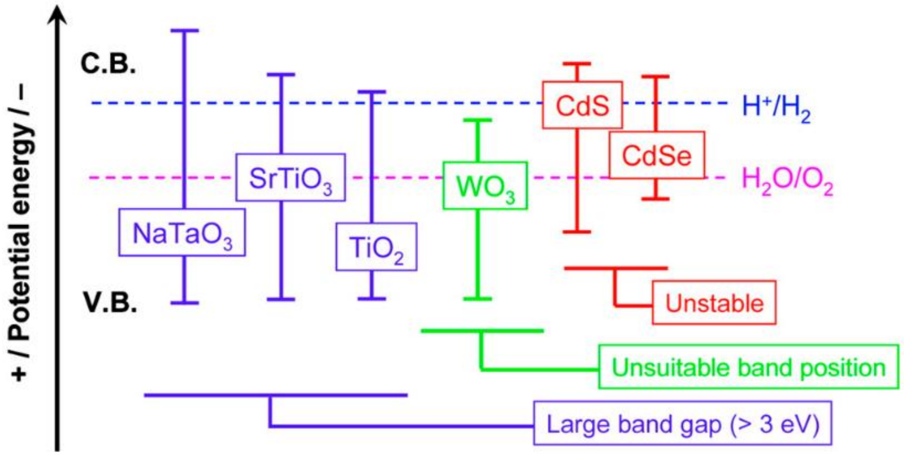

Figure 1.3 Band gap energies and band edge potentials of different photocatalytic materials.[10]

1.3 Electrospinning Technique

The previously mentioned limitations accompanied with the use of fossil fuels lead to the need to find alternative sources of energy that are renewable, sustainable, and environmentally friendly, such as, solar energy, nuclear power, geothermal energy, wind power, biofuel and biomass.[4,11–13] The increasing demands for materials that is efficient for such technologies resulted in expanding the research conducted on nanosized materials, especially one-dimensional (1D) nanostructures, such as nanotubes, nanowires, and nanofibers due to their unique properties.[3,11,14–16] Up to now, different techniques have been established to fabricate 1D nanostructures such as, template directed, hydrothermal, interface synthesis technique, lithography, chemical vapor deposition, focused ion beam writing, self-assembly, and electrospinning.[17] Nevertheless, most of these techniques have limitations, such as complexity, high cost, and material limitations. This attracted the attention to the electrospinning technique, as it is a simple and low-cost technique. Electrospinning technique is mainly used to fabricate nanofibers structure. It can be applied to metals and ceramics using natural and synthetic polymer alloys.[17,18] Modified electrospinning technique can also be used to fabricate hollow fibers, helix fibers, core-shell fibers, and porous fibers.

1.4 Scope of the Thesis

The aim of this study is to fabricate one-dimensional nanofibers of titanium and titanium-copper composites and study the effect of different annealing atmospheres (oxygen, air, and argon) on their crystal structure, band structure, absorption, and photocatalytic activity towards water splitting. The incorporation of CuO with its smaller band gap, would greatly enhance the light absorption characteristics of TiO_2. Also, the possibility to keep copper in its metallic state (zero oxidation state) is expected to enhance the photocatalytic water splitting activity of TiO_2.

Chapter 1 gives an overall idea about the increasing energy demand and the negative impacts caused by combustion of fossil fuels, also how to reduce carbon dioxide emissions in the atmosphere. The chapter also discusses the meaning of a photocatalyst, the restrictions of the material selected. Finally, it describes the concept of electrospinning.

Chapter 2 summarizes the scientific background needed for this thesis. The concept of photocatalytic water splitting is explained, why to use metal oxides nanostructures, the unique properties of TiO_2 and its limitations as a photocatalyst, and finally, doping and incorporating other metals, such as copper to enhance the utility of TiO_2.

Chapter 3 gives an overview of the recent literature on nanofibers for photocatalytic water splitting and the unique properties offered by the nanofibers structure.

Chapter 4 shows the experimental design used in the fabrication process starting from solution preparation, electrospinning, annealing in different atmospheres, and finally the characterization techniques used.

Chapter 5 discusses the first part of the thesis, concerning the fabrication of TiO_2-CuO composite nanofibers and their morphological, thermal and structural analysis. Besides, their optical, photocatalytic and photoelectrochemical behavior.

Chapter 6 discusses the second part of the thesis, which is Cu^0 nanoparticles/TiO_2 composite nanofibers for photocatalytic water Splitting. It includes morphological features, optical and structural properties of the composite, and finally the photocatalytic activity of the composite nanofibers for water splitting.

Chapter 7 presents the suggested strategies that can be applied to further improve the efficiency of the materials used as photocatalysts for water splitting.

Chapter 2

Background

2.1 Photocatalytic Water Splitting

2.1.1 Hydrogen Generation by Water Splitting

The water splitting process involves two main reactions as shown in Eq. 2.1, 2.2, and 2.3. According to thermodynamics, the process of water splitting is a nonspontaneous process, as the calculated Gibb's free energy for the two half reactions is positive ($\Delta G_{H2O}{}^{o} = 238$ kJ mol^{-1}).[8] Also, $\Delta E^0 = -1.23$ V vs SHE, where the negative value of ΔE^0 indicates that water splitting reaction is thermodynamically nonspontaneous. Thus, the system needs external energy to perform the required reaction, which can be provided by applying a bias of 1.23 V to enforce the reaction to proceed.[19]

$$\text{Oxidation: } 2H_2O \rightarrow O_2 + 4H^+ + + 4e^- \quad E^0 = 1.23 \text{ V vs SHE} \qquad (2.1)$$

$$\text{Reduction: } 2H^+ + + 2e^- \rightarrow H_2 \quad E^0 = 0.00 \text{ V vs SHE} \qquad (2.2)$$

$$\text{Overall: } 2H_2O + 2\,e^- \rightarrow 2H_2 + O_2 \quad \Delta\,E^0 = -1.23 \text{ V vs SHE} \qquad (2.3)$$

2.1.2 Water Splitting

The Electrolysis process mainly involves dissociating the bonded elements in a compound by applying a bias through them. In water electrolysis H_2O molecule is decomposed into oxygen and hydrogen gas. Usually the electrolytes should contain free ions for the medium to be electrically conductive. This setup used in this process is typically composed of two electrodes, anode (performs the oxidation reaction), and cathode (performs the reduction reaction). The main limitation with the electrolysis technique is that the electrons needed to perform the reaction is mainly provided using electricity, which is generated by combustion of fossil fuels, which is a nonrenewable source of energy and increases CO_2 emissions as explained previously in chapter 1.[8]

2.1.3 Photocatalytic Water Splitting

Photoelectrolysis mainly depends on the direct use of light to generate the electrons needed to perform the water splitting reactions using a semiconductor material. Thus, combining solar energy harvesting and water electrolysis in one single photoelectrode. As shown in Figure 2.1 the process of photocatalytic water splitting mainly involves a semiconductor, which is when irradiated with light (photons) that possess energy equal to or larger than the energy of the band gap of the used semiconductor, electrons from the valence band are excited to the conduction band forming what is known as an “e^--hole$^+$” pair. These photogenerated charge carriers diffuse to the surface of the semiconductor, to perform the desired oxidation/reduction reaction of water, as shown in Eq. 2.4, 2.5, and 2.6.[8]

$$2h\nu + \text{Semiconductor} \rightarrow 2h^+ + 2e^- \qquad (2.4)$$

$$2h^+ + H_2O\ (l) \rightarrow \frac{1}{2}O_2(g) + 2H^+ \qquad (2.5)$$

$$2H^+ + 2e^- \rightarrow H_2(g) \qquad (2.6)$$

2.1.3.1 Photoelectrochemical Cells

Photoelectrochemical cell is typically formed of three electrodes, a cathode, anode, and a reference electrode, at least one of the electrodes used is a semiconductor, which is called a photoelectrode, these electrodes are immersed in an electrolyte. When the incident solar energy is absorbed by this photoelectrode, current and voltage is generated. Usually an n-type semiconductor is used as a photoanode, on which oxygen evolution takes place, while hydrogen evolution takes place at the cathode, which can be a metal or a p-type semiconductor (photocathode).[8]

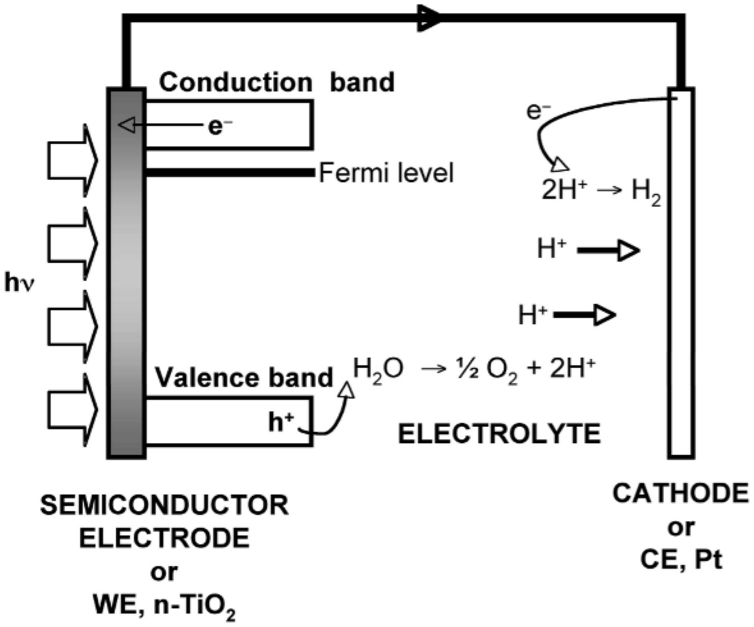

Figure 2.1 Illustration of photocatalytic water splitting using a photoelectrochemical cell.[8]

During the past few decades, various fabrication methods have been introduced to synthesize different nanostructures. Thus, researchers have been trying to explore different structures to determine which structure possesses the most promising properties to give the highest hydrogen yield. Many of these nanostructures are in the form of powders, like the one we are discussing in this thesis. The main advantage of using photocatalysts in the form of powder in water splitting is simplicity, as shown in Figure 2.2

Photocatalytic water splitting by powdered photocatalyst.[21] The powdered photocatalyst is suspended in the electrolyte, the reactor is then irradiated with Sun light, and hydrogen is easily obtained. The limiting issue with the use of powdered photocatalyst is the limited separation of the evolved H_2 and O_2. However, the problem can be solved by using a Z-scheme photocatalyst system. Moreover, powdered photocatalyst is more promising on an industrial scale due to its simplicity.[20]

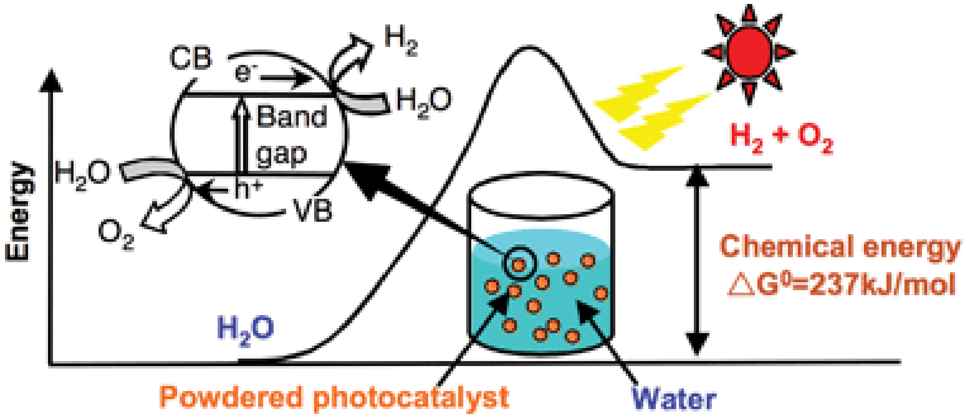

Figure 2.2 Photocatalytic water splitting by powdered photocatalyst.[21]

2.1.3.2 Structural Properties of the Photocatalyst

For efficient photoelectrochemical water splitting, the material used as a photoelectrode must satisfy the following requirements. The semiconductor valence band and conduction band must be aligned with the redox potential of the water, for the electrons and holes to transfer from the conduction band and valence band of the semiconductor to perform the desired redox reactions. It should also be stable in wide range of pH, to resists dissolution and photocorrosion. Besides, it should offer high charge transfer rate to avoid charge recombination, charge accumulation, or corrosion of the electrode itself. Finally, the band gap should not be very large for the semiconductor to absorb most the solar spectrum.

2.2 Metal Oxides (Ceramics) as Photoanodes

Metal oxide semiconductors have the advantage of being stable comparing to non-oxide semiconductors and relatively cheap. After the first study conducted of Fujishima and Honda, where they used n-type TiO_2 as a photoanode for photocatalytic water splitting. Other metal oxides with different structures have been investigated as photoanodes. Metal oxides showed high stability and reasonable charge transfer properties. However, the main obstacle holding the applicability of photocatalytic water splitting is that researchers are still looking for a semiconductor that possesses narrow band gab to be able to harvest most of the solar spectrum and stable at the same time, as most of the materials explored have only one of the two characteristics. Although narrow band gap semiconductors absorb most of the solar radiation, they are easily corroded under illumination. On the other hand, materials with wide band gap show high stability against photocorrosion but absorbs only in the UV range of the solar spectrum, which is almost 4-5% of the solar radiation.[8]

2.3 Nanostructures Properties-Large Surface to Volume Ratio (Surface Activities)

Unlike the charge separation process in bulk materials, which is strongly affected by the electric field formed at the depletion layer at the interface between the electrolyte and the bulk semiconductor, charge transfer in nanocrystalline semiconductor occurs via diffusion from the interior to surface traps, as band bending is small. Semiconductor nanoparticles have the advantage of having significantly short diffusion lifetime (τ_d), of the generated charges from bulk to the surface, compared to recombination time (τ_r) of the electron-hole.[8,22] As the particle size increases, τ_d becomes almost equal to τ_r, at the size of 1 μm, electron-hole recombination rate starts to be higher than surface diffusion phenomena. Since the rate of charge carrier diffusion is higher than the rate of electron-hole recombination, if one of the photogenerated charge carriers is captured from the surface, a quantum yield approaching unity can be achieved.[22]

2.4 Titanium Dioxide (TiO_2)

2.4.1 Crystal Structure of TiO_2

There are three crystalline phases of TiO_2, which are anatase (tetragonal), brookite (orthorhombic), and rutile (tetragonal), as shown in Figure 2.3 The crystal structures of TiO_2 anatase (tetragonal) polymorphs, rutile (tetragonal), and brookite (orthorhombic).[25]. In all three phases, titanium cations are coordinated to six oxygen anions, resulting in distorted TiO_6 octahedra structure. The anatase structure is formed by sharing the corner of TiO_6 octahedra, while rutile structure is formed by sharing the edges of the octahedral, for the brookite structure TiO_6 octahedra is joined by sharing both the corner and the edges of the octahedral.[23] Anatase has a tetragonal a=0.536 nm and c=0.953 nm (anatase), rutile have a tetragonal structure with a=0.459 nm and c=0.296 nm. Brookite structure possesses an orthorhombic structure with a=0.915 nm, b=0.544 nm, and c=0.514 nm. Rutile is considered the most stable phase in bulk TiO_2. However, at the nanoscale, anatase and brookite possess lower surface energy, and therefore are considered more stable at the nanoscale, there are still some debates in literature on this point.[24]

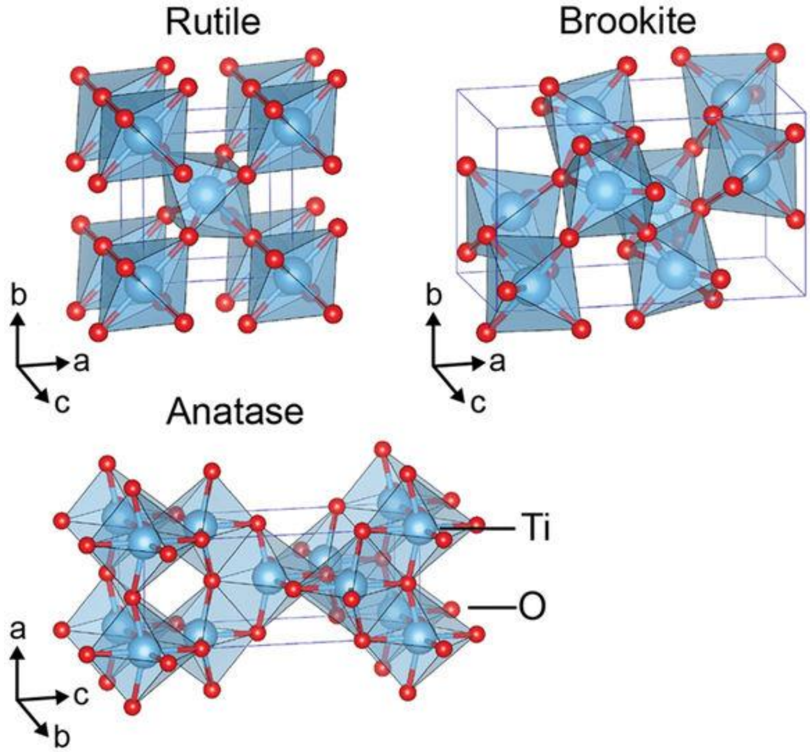

Figure 2.3 The crystal structures of TiO_2 anatase (tetragonal) polymorphs, rutile (tetragonal), and brookite (orthorhombic).[25]

2.4.2 Limitations of Using TiO_2 as a Photocatalyst

TiO_2 is One of the most widely investigated materials in hydrogen generation applications, as it is an earth abundant element, low cost, stable and has high photocatalytic activity. However, one of the major limitations is its wide bandgap of TiO_2, 3.2 eV for the anatase phase and 3.0 eV for the rutile phase. This limits its absorption to the UV range of the solar spectrum. Besides suffering from high rate of charge recombination. Doping TiO_2 with other metals or narrow band gap semiconductors is one way to narrow its bandgap and enable it to absorb wider range of the solar spectrum.[17] Also the electric field formed due to the presence of a heterojunction facilitates charge separation and lowers the rate of charge recombination.[24]

2.4.2.1 Wide Bandgap

Although TiO_2 fulfils many of the requirements of an efficient photocatalyst for water splitting application. Such as, stability against photocorrosion, non-toxicity, and reasonable cost. It is absorption is still limited by its wide band gap (3.0 to 3.2 eV), various techniques have been proposed to increase the absorption of TiO_2 to the visible region of the solar spectrum. Including, coupling with narrow band gap semiconductor, dye sensitization, and doping.[26]

2.4.2.2 Electron-Hole Recombination

Another limiting Factor is the recombination of the photogenerated charge carriers.[26] Which is usually caused by bulk or surface defects or the impurities present in the material.[27,28] This problem can be treated by incorporating species that can promote charge separation. This has been explored using different modifiers such as, other semiconductors[29,30], noble metals[31,32], and ions[27,33].

2.4.3 Doping

As discussed in the previous section doping is a very promising solution that can be applied to overcome some of the limitations that encounters TiO_2 from being an efficient photocatalyst for water splitting reaction.[17] In this regard, doping with noble metals was shown to be very effective in enhancing the photocatalytic activity of TiO_2. However, noble metals are very expensive and not earth abundant. Thus, finding alternative cost-effective materials is very crucial.[34] On the other hand, blending TiO_2 with other semiconductors of smaller band gap to extend the absorption to a wider range of the solar spectrum was investigated.[35] According to previous studies CuO seems to be a promising candidate due to its narrow bandgap (1.4-1.6 eV)[34–43] which enables it to shift the absorption range to the visible region of the solar spectrum.

2.5 p-n Heterojunction

There are three types of heterojunctions that can be formed, depending on the band positions of the two semiconductors, as shown in Figure 2.4. Type II is considered the most suitable condition for efficient separation of charge carriers. As electrons become more stable energetically when they are transferred from the higher conduction band to the lower conduction band, while holes move in the opposite direction from the lower valence band to the higher valence band. At the end electrons and holes are separated and move in opposite directions. Resulting in an increase in the charge carriers' life time and reduces the recombination rate. This configuration is expected to be the one describing CuxO/TiO_2 system, Besides the formation of an internal Electric field at the interface between the n-type semiconductor and p-type semiconductor, resulting in band bending phenomena due to charge accumulation at the interface.[44] Figure 2.5 illustrates the mechanism of charge transfer in CuO/TiO_2 heterojunction.[45]

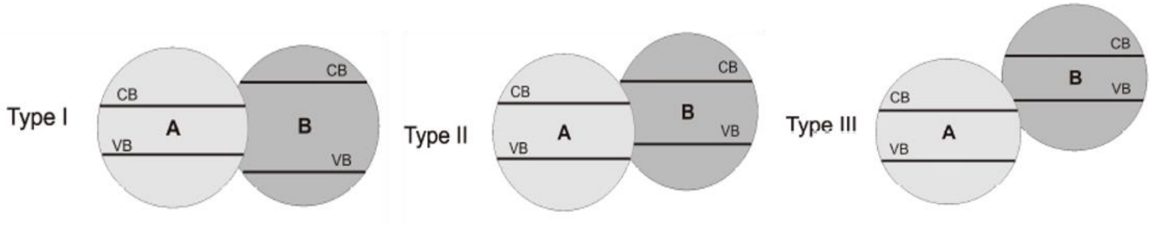

Figure 2.4 Different types of heterojunction systems.[46]

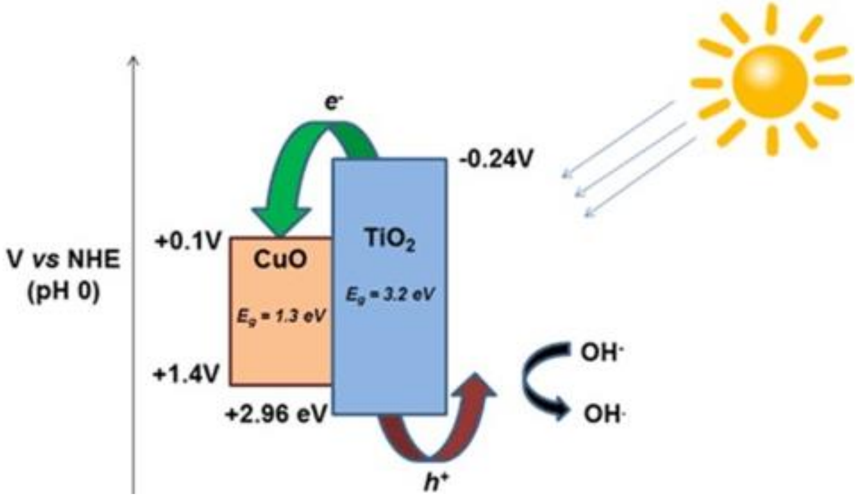

Figure 2.5 Mechanism of charge transfer in CuO/TiO_2 heterojunctions.[45]

2.6 Metallic Copper and Plasmonic Photocatalysis

TiO_2 modified with metallic copper nanoparticles is very promising in UV and visible light-induced photocatalytic reactions. Cu NPs can act as an electron sink and inhibit the recombination of the photogenerated charge carriers.[46] As the conduction band of TiO_2 is above the Fermi level of metallic Cu, the photogenerated electrons can be easily transferred from TiO_2 to Cu NPs. Besides Cu NPs can activate TiO_2 towards the visible light region of the solar spectrum using localized surface plasmon resonance (LSPR) of Cu.[47–52] The LSPR effect is activated when light interacts with the free electrons of the metallic nanostructure, resulting in oscillations (collective excitations), these oscillations significantly improves the local electromagnetic field around the nanoparticles.[53] Spherical metallic nanoparticles made of silver, gold, and copper, are relatively smaller than the wavelength of the light, thus it is resonant with the incident light, and an enhancement in the local electromagnetic field on the particle surface is observed.[46]

This characteristic surface plasmon resonance band that absorbs light in the visible region shifts the absorption of noble metal modified titanium dioxide towards the visible region. This could be understood in terms of the efficient transfer of the photogenerated electrons from the metal to the conduction band of TiO_2, as shown in Figure 2.6. Thus, TiO_2 becomes electron-rich, while the metal becomes electron-deficient. therefore, the photocatalytic oxidation reaction takes place on the surface of the metal rather than the surface of TiO_2.[54] Due to the superior properties of LSPR, many studies were conducted on Ag and Ag to study their plasmonic behavior. However, the plasmonic effect of copper and its effect when Cu nanoparticels are combined with TiO_2, is not widely covered so far. This is due to the fact that metallic copper (zero-valent) is very hard to maintain in zero oxidation state.[55–57]

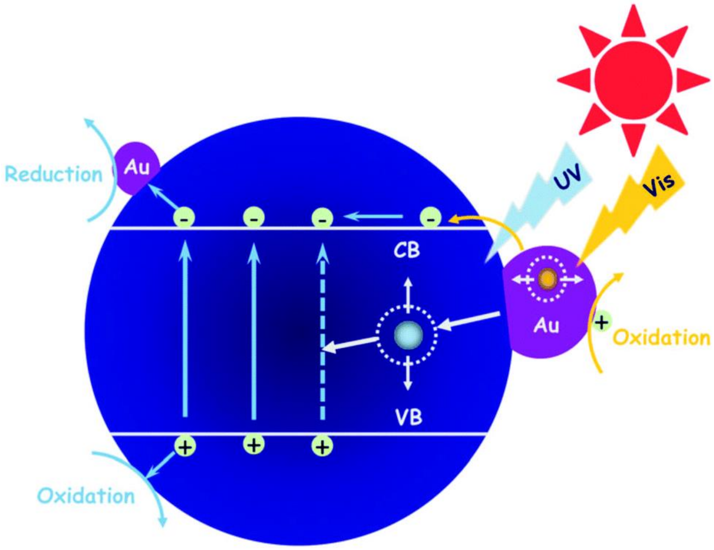

Figure 2.6 The effect of gold particles in promoting the photocatalytic activity of TiO_2 under UV-visible light irradiation.[53]

2.7 Graphene

Graphene consists of a sheet with the thickness of one-atom, formed of an sp^2-bonded carbon structure.[58] Offering superior quality of electronic and crystal structure.[59–62] Previous studies suggest that the specific surface area of a single layer of graphene is almost 2630 m^2/g.[63,64] besides its significant electronic conductivity.[65,66]

2.7.1 Graphene-Copper Composite

Studies have shown that due to graphene having characteristic 3-D folded structure and large surface area, it is an excellent carrier for copper nanoparticles.[67] As copper gets adsorbed on the surface of graphene, thus hinders the agglomeration and oxidation of copper.[68,69] At the same time, when copper nanoparticles is adsorbed on the surface of graphene, it weakens the π - π interaction among the graphene sheets. Thus, it reduces the stacking of graphene sheets.[70]

2.8 Electrospinning Technique

The idea of electrospinning mainly depends on the electrostatic attraction of a liquid, which was reported by William Gilbert, he observed that when an electrically charged piece of amber is brought close to a droplet of water, the droplet forms a cone shape and small droplets are ejected from the tip of the cone.[71]

2.8.1 Electrospinning Basic Principles

A typical electrospinning setup consists of three major parts: a power supply (high voltage source), a metallic capillary tip, and a collector as shown in Figure 2.7. The syringe contains a polymer solution, the solution is usually fed through the spinneret at a constant and adjustable rate using a syringe pump, and a high voltage usually 10 to 50 kV is applied between the collector and the syringe tip.[18,72] When the solution is subjected to high voltage, it becomes highly charged, thus, the solution droplet at the tip suffers from two opposite forces, surface tension and the electrostatic repulsion force. these electrostatic interactions result in the formation of a conical fluid at the tip of the syringe, this structure is called the “Taylor Cone”.[18,73,74] At a specific voltage, the electrostatic repulsion force formed on the charged polymer overcomes the surface tension of the solution, and a charged jet is ejected from the tip of the formed Taylor Cone, moving towards the counter electrode, and the solvent starts to evaporate. At the end solid fibers are collected on the counter electrode, with diameters ranging from nanometers to micrometers.[17]

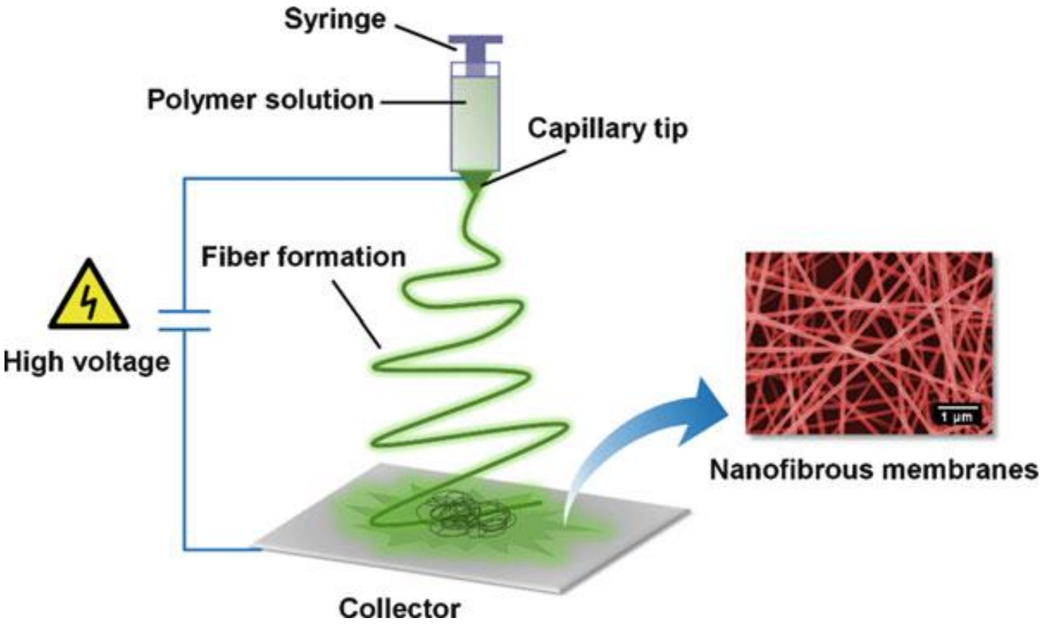

Figure 2.7 Schematic illustration of the basic setup for electrospinning. The inset shows SEM image of the PA6 nanofibrous membranes deposited on the collector.[170]

2.8.2 Controlling Parameters of the Electrospinning Process

There are mainly three types of parameters that can be changed to control the electrospinning process, which are: ambient parameters including the temperature and the humidity percentage in the surrounding atmosphere. Process parameters include applied electric field, feed rate, and the distance between the tip and the collector. Finally, solution parameters include conductivity, viscosity, surface tension, and molecular weight. The diameter of the fabricated nanofiber is easily adjusted by varying these parameters.[14,75]

2.8.2.1 Solution Parameters

i. Polymer Concentration and Viscosity

The viscosity of the solution is directly proportional to the concentration of the polymer in the solution. The molecular weight of the polymer, the temperature and the solvent properties also effects the viscosity of the solution. There is a minimum polymer concentration needed for the solution to spin, at high concentrations, the formed fibers are not continuous as the solution flowing to the tip is not constant.[14,75]

ii. Conductivity

A key factor in initiating the process of electrospinning is that the solution must be charged with the voltage that enables the repulsive forces in the solution to overcome the surface tension of the solution. The conductivity of the solution also affects the elongation and stretching of the resultant jet.[17] If the conductivity of the solution is low, this result in insufficient stretching of the fiber and there might be some beads in the resulting fiber, while if the electric conductivity is high this result in reducing the diameter of the obtained nanofibers.[14] The conductivity of the solution is determined by the type of the polymer, the salt, and the solvent sort.[17] Natural polymers are generally polyelectrolytic, the presence of ions in the solution increases the capacity of charge carrying, this result in higher tension with the electric field. This makes fabricating the fiber using synthetic polymer easier than a natural polymer like gelatin for instance.[17]

iii. Surface Tension

High surface tension might encounter the spinning process if it is larger than the charge in the solution. Besides, it might result in droplets formation.[14] It was found that surface tension is inversely proportional to the elongation of the charged jet, if the surface tension of the solution decreased this enables the electrospinning process to occur at lower voltages.[17,76]

2.8.2.2 Processing Parameters

i. Applied Voltage

Applying a high voltage (higher than 6 KV) is very essential to initiate the electrospinning process, as it induces charges in the solution, that strengthen the electrostatic force in the solution and overcomes the surface tension. Finally, a Taylor cone is formed. It was found that increasing the voltage decreases the diameter of the fiber.[11,14] However, this behavior is also affected by the distance between the collector and the tip and the concentration of the solution.[17]

ii. The Distance between the Tip and Collector

There is an optimum value of the distance between the collector and the tip for each electrospinning system, below which the solvent will not have enough time to be evaporated and the strength of the electric field will be very high. This may lead to the presence of unevaporated solvent in the fiber. If the distance is very long the electrostatic field strength is decreased, thus the fiber diameter increases as the elongation of the fiber decreases.[14,77]

iii. Feed Rate

This factor determines the amount of the solution reaching the tip per unit time. The feed rate is directly proportional to the diameter of the fiber and the size of the beads, a minimum value of the feed rate is required to initiate and maintain the process of electrospinning. Usually, as the feed rate increases, the fiber diameter and beads size increase.[17]

iv. Humidity

When the electrospinning process is performed at high humidity, water vapor is condensed on the fiber, this might affect the morphology of the fiber, especially when the solvent used is volatile. The porosity of the fiber and the size of the pores formed increases as humidity increases. Humidity affects solvent evaporation rate, if the humidity is very low this might lead to clogging the tip of the needle at a very brief time due to rapid evaporation of the solvent.[78]

2.9 Ceramic Nanofibers

Ceramic nanofibers can be easily prepared from the ceramic precursors using the electrospinning technique followed by calcination of the electrospun nanofibers to obtain the ceramic nanofibers. The strong covalent and ionic bonds present in ceramic materials makes the ceramic structure resists chemical corrosion, tolerates high temperatures, and its surface adsorbs foreign species. However, this also makes ceramics brittle due to their weak mechanical properties.[17]

Chapter 3

Literature Review

3.1 Electrospun Nanofibers for Photocatalytic Water Splitting

3.1.1 Narrowing the Bandgap of TiO_2

As stated before, TiO_2 suffers from having a wide bandgap. In this regard, Babu et.al synthesized N-doped TiO_2 nanostructures using electrospinning technique combined with solgel method and they found that the bandgap of N-doped TiO_2 was reduced to 2.83 eV, which was confirmed by an increase in the H_2 evolution rate by about 12 times that of pristine TiO_2. This enhancement in the photocatalytic activity of TiO_2 was attributed to the larger surface area of the nanostructure and the narrower band gap.[79]

3.1.2 Enhancing Charge Transfer

Another obstacle is the recombination of the generated electron-hole pair. This problem can be solved by incorporating materials that are highly conductive to capture the generated electron before it recombines with the hole. An example of this is the electrospun TiO_2/SnO_2 nanofibers that were fabricated by lee et.al. They found that the sample with 3% Sn gave the highest H_2 evolution rate. The large surface area of nanofibers is a major advantage of nanofibers over other nanostructures.[80]

This concept was confirmed by the same group, where they fabricated a “Forest like” structure by fabricating TiO_2 nanofibers, which were used as the trunk, then using hydrothermal techniques they grew ZnO nanorods as the branches, finally copper nanoparticles were photodeposited on the structure acting as the leaves. The hierarchical nature of this structure gave higher surface area, hence better light absorption. There was an enhancement in charge separation due to the coupling of different semiconductor materials.[81]

3.1.3 Surface Area

A comparison was made by Choi et.al between electrospun TiO_2 (prepared using a suspension of TiO_2 nanoparticles) and TiO_2 nanoparticels. It was found that mesoporous nanofibers structure has larger surface area, hence it provides more active sites for water molecules to get adsorbed on the surface. This resulted in an overall increase in the photocatalytic activity, as the photocurrent of the nanofiber structure was found to be almost 3 times that of the nanoparticles structure. This was explained in terms of higher surface area due to the porous structure and they found that the nanofiber structure made the nanoparticles densely packed which increased the interconnection between the nanoparticles, resulting in better charge separation.[82]

3.1.4 TiO_2-CuO Composite

Previous studies have shown that incorporating CuO as a co-catalyst with TiO_2 can greatly enhance the efficiency of photocatalytic water splitting. Bandara et al. fabricated TiO_2/CuO catalyst, which showed very high catalytic activity, due to the accumulation of the excited electrons from both CuO and TiO_2 in the conduction band of CuO, thus the fermi level of CuO was shifted upwards, giving the overvoltage needed for water splitting.[39] TiO_2 nanotubes decorated with CuO were fabricated by Xu et al., exhibiting hydrogen rates of around 64.2-71.6 mmolh^{-1}g^{-1}.[38] However, the poor photostability of copper oxides limits their use as a co-catalyst in photocatalytic reactions.[46] The amount of hydrogen reported so far is still far below the theoretical limit of photocatalytic water splitting. On the other hand, CuO_x/TiO_2 composite is mostly investigated in the form of nanoparticles, which suffer high recombination rates at the grain boundries.[34]

As an emerging structure, nanofibers have been investigated by Einert et al. using fibrous CuO as a photocathode for photocatalytic water splitting.[9] However, the stability of the electrode was still a limiting issue.[83] Also, Hou et al. fabricated electrospun TiO_2/CuO/Cu mesoporous nanofibers combined with a foaming agent.[5] These electrodes exhibited photocatalytic H_2 yield of almost 851.3 μmol g^{-1} h^{-1}. The authors attributed this enhancement to the presence of a heterojunctions at the TiO_2/CuO, and CuO/Cu interfaces, resulting in more efficient charge carriers separation.[37]

Herein, we report on the optimized fabrication of electrospun TiO_2-CuO composite nanofibers. The nanofiber composites were annealed in different atmospheres and the most photoactive crystalline phase was identified. Also, the effect of different CuO loading as a co-catalyst on the optical and photocatalytic water splitting performance was demonstrated.

3.1.5 Limitations of Copper Oxides in Photocatalysis

Both oxide forms of copper, CuO and Cu_2O are p-type semiconductors with band gap energies of 1.5 eV and 2.1 eV, respectively. Both are very promising as a photocatalyst in water splitting.[84–87] However, they suffer from not being a photostable material. As CuO possesses smaller band gap, it absorbs larger amount of the visible spectrum of the solar radiation. Some studies suggest that the co-existence of CuO and Cu_2O can enhance their stability and be more efficient than using each of them solely.[88]

3.1.6 Metallic Copper as a Co-catalyst

According to previous studies.[34–38,41,89,90] copper seems to be very promising as a co-catalyst with TiO_2. This is due to copper being an earth abundant element, unlike noble metals, which are rare. Besides, copper is in the same group in the periodic table of silver and gold with similar crystal structure, face centered cubic (FCC), and similar electronic configuration. This leads us to believe that there is a great potential to enhance the photocatalytic activity using TiO_2 modified with copper.[46] Copper can exist in different oxidation states: Cu^0, Cu^{+1}, Cu^{+2} and Cu^{+3}. Copper species that are promising in increasing the photocatalytic activity of TiO_2 are metallic copper, Cu_2O, and CuO.[46] Although metallic copper is very promising, especially that it shows plasmonic activity close to that of gold and silver. However, developing an applicable technology that can be used to maintain copper in zero-valent oxidation sate is still an obstacle, and intensive research is being conducted to solve this issue.

3.2 Stabilizing Metallic Copper

Copper metal shows excellent thermal and electrical properties, besides its low cost. However, it is very hard to maintain it in the metallic form, as it is easily oxidized to CuO or Cu_2O when exposed to air. Therefore, many studies have been performed to prevent its oxidation by minimizing the contact between copper and air.[91] Different approaches have been investigated to overcome this problem. Such as polymers,[92–97] and metallic coatings.[92,98–101] The thickness of polymeric coatings strongly affects the properties of the coated metal.[91,102]

Many studies have been conducted recently to fabricate protective coatings made of graphene, as it is chemically stable, besides having higher thermal mobility and electrical conductivity than copper.[94,103,104] Most of the previous studies mainly involved coating copper metal with graphene using chemical vapor deposition (CVD) technique.[102,105] However, using CVD involves using a gas source, which requires a temperature of almost 1000 °C, thus limiting the number of transition metals that can be used. Other studies used polymers such as PS, PMM, and PVP as solid carbon sources for graphene preparation.[91,106,107] Using solid carbon source has the advantage of reducing the temperature needed for the process.[106–108]

Chapter 4

Materials and Experimental Methods

4.1 Nanofibers fabrication

4.1.1 Materials

Titaniumisoprorpoxide, copper(II) acetate monohydrate ($C_4H_6CuO_4 \cdot H_2O$), Polyvinylpyrrolidone (PVP, Mw ≈ 1300 000), ethanol absolute, acetic acid. All chemicals were purchased from Aladdin. All chemicals were used directly without further purification.

4.1.2 Solution Preparation

Titanium nanofiber and titanium-copper composite nanofibers were fabricated using the electrospinning technique. For titanium nanofibers, a solution consisting of 0.5 gm of titanium isoprorpoxide was added to 4 gm of (Polyvinylpyrrolidone) PVP 10% (The PVP solution was made using PVP and ethanol absolute as polymer and solvent, respectively), and 1 gm acetic acid, finally the solution was stirred for 2 hours.

For copper nanofibers different weights of copper acetate monohydrate (0.05, 0.075, 0.1, and 0.125) were dissolved in 2.5 gm of ethanol absolute, the solution was stirred for 2 hours at 80 °C, after copper acetate was completely dissolved, the heat was turned off and 0.25 gm of PVP and 5 gm of acetic acid were added to the solution, the mixture was stirred until the polymer is completely dissolved. Finally, to prepare the titanium-copper composite nanofibers, the two solutions previously mentioned were mixed with continuous stirring till complete homogeneity.

4.1.3 Electrospinning

The diameter of the fabricated nanofibers was optimized by changing the applied voltage and the feed rate. Different voltages (14 to 21 KV) and different feed rates (3.9 to 4.5 ml/h) were chosen for comparison.

Chosen Parameters

After trying different voltages and feed rates. The following parameters were chosen for during the fabrication process of the nanofibers studied in this thesis. The distance between the syringe tip and the grounded aluminum foil collector was fixed at 15 cm. The voltage was fixed at the range of 19 to 21 kV, and the feed rate was in the range 4 to 4.5 ml/h, at humidity of (35 ± 5%). Each of the prepared solutions was passed through the syringe with a 1.1 mm diameter stainless steel nozzle (Li and Xia, 2003).

4.1.4 Annealing

The electrospun nanofibers were annealed in a Lindberg/Blue M tube furnace (model number: TF55030C-1) in air or oxygen atmospheres at 450 ◦C (1 deg/min) for 2 hours, and in argon atmosphere at 600 ◦C (2 deg/min) for 4 hours. Table 4.1 Coding of the fabricated titanium and titanium-copper composite nanofibers annealed in air and oxygen atmospheres.summarizes the details of the fabricated titanium and titanium-copper composite nanofibers annealed in different annealing atmospheres.

Table 4.1 Coding of the fabricated titanium and titanium-copper composite nanofibers annealed in air and oxygen atmospheres.

Titanium isopropoxide (g)	Copper acetate (g)	Annealing Atmosphere	Sample ID
0.5	0	O_2	O1
	0.05		O2
	0.075		O3
	0.1		O4
	0.125		O5
0.5	0	Air	A1
	0.05		A2
	0.075		A3
	0.1		A4
	0.125		A5
0.5	0	Ar	R1
	0.05		R2
	0.075		R3
	0.1		R4
	0.125		R5

4.1.5 Characterization

The morphology of the fabricated nanofibers was characterized with Zeiss SEM Ultra 60 field emission scanning electron microscope (FESEM), and High-resolution transmission electron microscopy (HRTEM).

The thermal stability of the fabricated nanofibers was characterized using TGA NETZSCH STA 409 C/CD apparatus under air. The crystal structure was identified using PANalytical X'pert Pro PW3040 MPD X-Ray Diffractometer (XRD) using copper CuKα radiation (λ= 0.15406 nm) in the range of 5° to 80° at a scan rate (2θ) of 3^{o} s^{-1} and was further confirmed using Raman microscope (Pro Raman-L Analyzer) with an excitation laser beam wavelength of 532 nm. Fourier transform infrared (FTIR) was also used to perform elemental analysis.

The absorption spectra of the nanofibers were recorded on a Lambda 950 UV/Vis spectrometer, EPR measurements were performed using Bruker EMX 300 EPR spectrometer (Bruker BioSpinGmbH, Silberstreifen 4, Germany).

Photoelectrochemical measurements were performed in a three-electrode cell, glassy carbon electrode loaded with the nanofiber was used as the working electrode, while platinum foil was used as the counter electrode, and saturated calomel electrode (SCE) as the reference electrode in 1 M KOH. A 300 W ozone-free xenon lamp and an AM 1.5 G filter at 100 $mWcm^{-2}$ were used to simulate Sunlight. And a scanning potentiostat (Biologic SP-200) was used to measure the photocurrent densities.

The photocatalytic activity of the fabricated nanofibers was tested in an inner-irradiation quartz annular reactor with a 300 W xenon lamp (CEL, HUL300), a vacuum pump, a gas collection, a recirculation pump, and a water-cooled condenser. 0.1 g of the sample was suspended in 1 M KOH using ultrasonic oscillator. Then the mixture was transferred into the reactor and deaerated by the vacuum pump. The xenon lamp was utilized as a light source, and the cooling water was circulated through a cylindrical

Pyrex jacket located around the light source to maintain the reaction temperature. The reactor was sealed with ambient air during irradiation, and the hydrogen evolution was monitored using an online gas chromatograph (GC, 7900) equipped with a Porapak-Q column, high-purity nitrogen carrier, and a thermal conductivity detector (TCD).

Chapter 5

TiO$_2$-CuO Composite nanofibers for Photocatalytic Water Splitting[†]

5.1 Nanofibers Optimization

i. Voltage

As shown in Figure 5.1, as the voltage increases from 14 to 17 KV, with a fixed feed rate of 4.1 ml/h, and fixing the distance at 15 cm, there was a decrease in the diameter of the fabricated fiber from 1.84 µm to 433 nm.

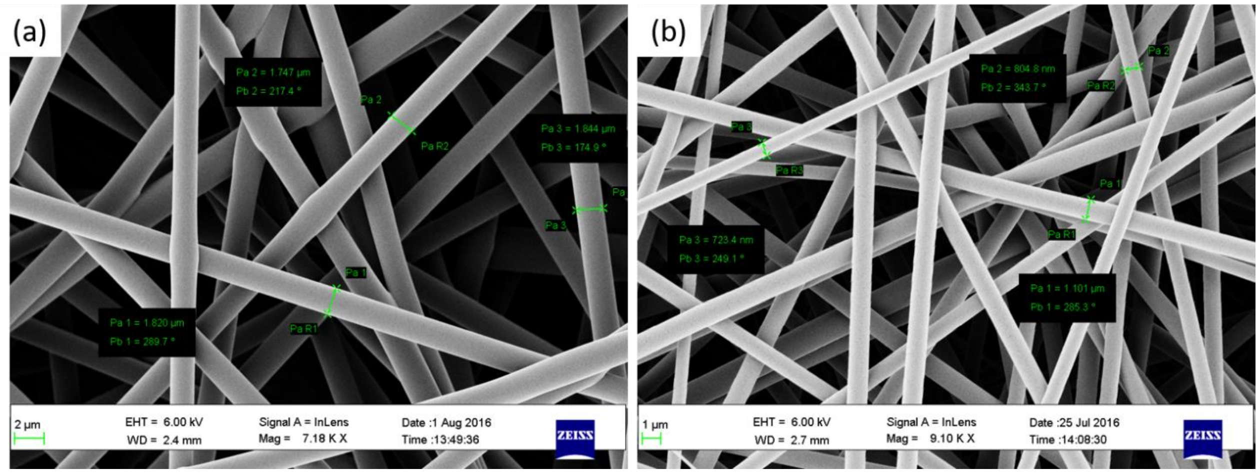

Figure 5.1 FESEM images illustrates the change in the diameter by changing the voltage applied, (a) at 14 KV, (b) at 17 KV.

[†] This Chapter has been submitted for publication: Menna M. Hasan and Nageh K. Allam, Unbiased Spontaneous Photocatalytic Water Splitting using Stable Erath Abundant Composite Nanofibers.

ii. Feed rate

Fixing both the voltage at 16 KV, and the distance at 15 cm, it was found that by increasing the feed rate from 3.9 to 4.3 ml/h, the diameter of the fabricated nanofiber also increased from 1.4 µm to 2 µm, as shown in Figure 5.2.

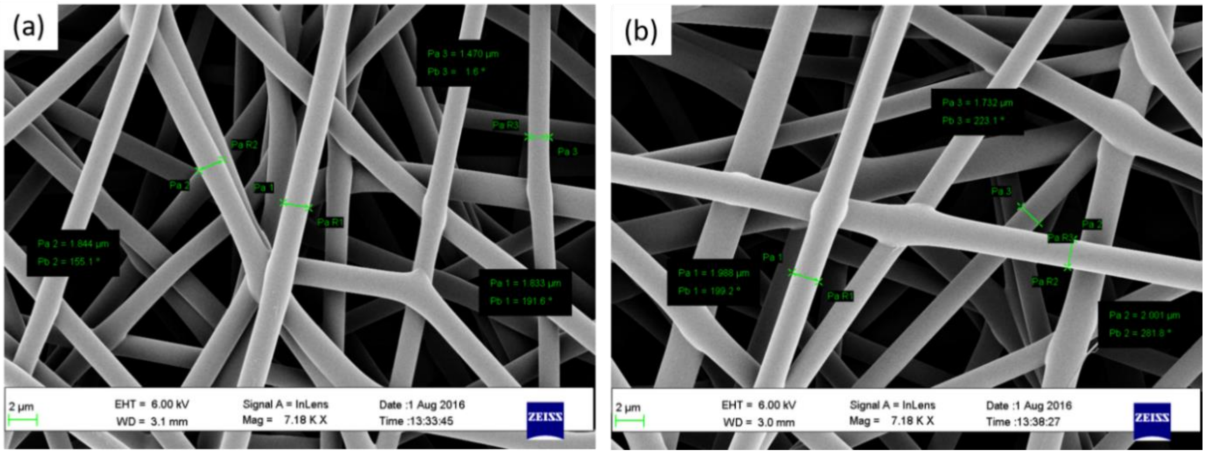

Figure 5.2 FESEM images illustrates the change in the diameter by changing the feed rate, (a) at 3.9 ml/h, (b) at 4.3 ml/h.

5.2 Morphological Features

Figure 5.3 shows FESEM images of the fabricated nanofibers before and after annealing for the air annealed samples. The as-electrospun TiO_2 nanofibers were smooth and highly dense with diameters ranging from 1.594 µm to 2.254 µm, Figure 5.3. Upon annealing in air atmosphere, the diameters were reduced to 180±10 nm, see Figure 5.4. While the Cu nanofibers completely collapsed upon annealing in air (Figure 5.3e), the TiO_2-CuO composite nanofibers maintained their morphology (Figure 5.3f) even with the highest copper concentration, see Figure 5.4.

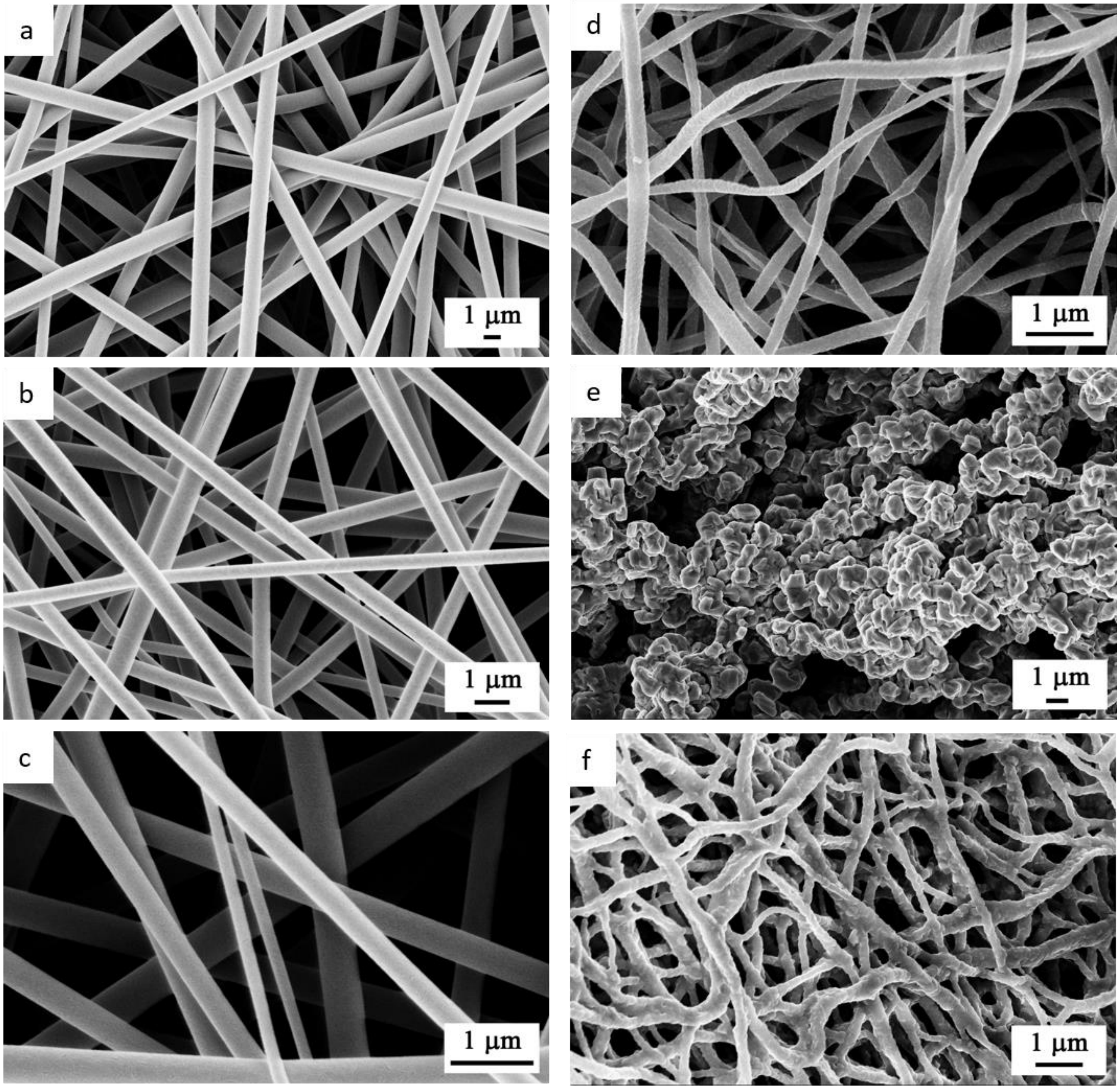

Figure 5.3 FESEM images of the electrospun (a) Ti NFs, (b) Cu NFs, (c) Ti+Cu composite NFs before annealing, (d) TiO_2 NFs, (e) CuO NFs, (f) TiO_2+CuO NFs composite after annealing in air atmosphere.

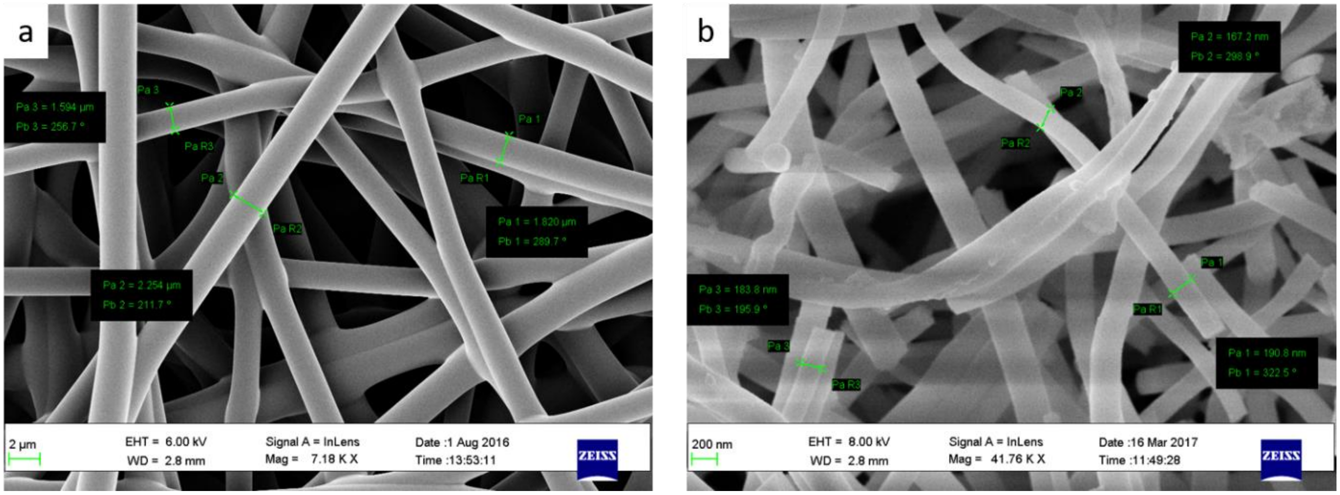

Figure 5.4 FESEM images illustrates the change in the diameter of TiO_2-CuO composite nanofiber, (a) before annealing, (b) after annealing.

5.2.1 Thermal Analysis

Figure 5.5 shows the TG analyses of the fabricated TiO_2 and TiO_2-CuO composite nanofibers. Four major weight loss steps can be identified in the TG graph of TiO_2 nanofibers. The weight loss (2.78%) below 100 °C can be attributed to the evaporation of the residual moisture or any possible residual traces of the solvent (ethanol). The weight loss between 100 °C and 320 °C (3.11%) can be ascribed to the decomposition of the side chain of PVP. The steep slope in the range 320 - 470 °C involves a weight loss of 54.52% and can be related to the degradation of the main chain of PVP. The final step involves the conversion of the as-spun titanium oxide nanofibers into the anatase phase.[109–111] In contrary, the TG analysis for the TiO_2-CuO composite nanofibers showed a small weight loss of almost 20% in the temperature range 40 - 200 °C, which can be related to the evaporation of moisture and any residuals from the solvent. Note the major weight loss (65.5%) in the temperature range 230 - 370 °C, which can be related to the degradation of the polymer (PVP). [112] No further weight losses were observed up to 800 °C.

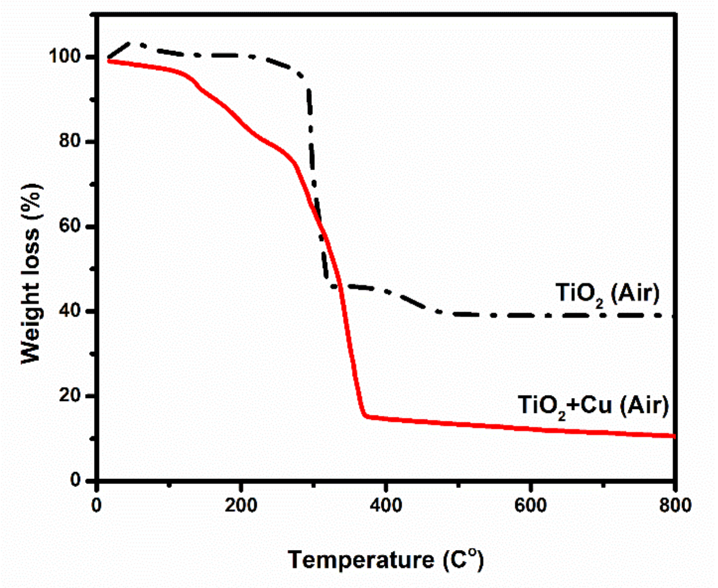

Figure 5.5 TG curves of thermal decomposition of as-spun TiO_2 and TiO_2-CuO composite nanofiber nanofibers in air.

5.3 Structural and Elemental analysis

Figure 5.6 shows the XRD patterns of the fabricated nanofibers annealed in different atmospheres. The XRD pattern of TiO_2 nanofibers annealed in air showed three dominate diffraction peaks at 2Θ = 25.4°, 37.2° and 48.2°, corresponding to (101), (004), and (200) facets of the anatase phase, respectively.[113,114] However, upon annealing the TiO_2 nanofibers in oxygen, the peaks were observed at 2Θ = 27.4°, 36°, and 41°, corresponding to (110), (101), and (111) facets of the rutile phase, respectively. In oxygen-rich atmosphere there is a large number of adatoms that react instantly with interstitial Ti^{3+} on the surface forming TiO_x islands, which act as rutile islands, resulting in a very high rate of phase transformation at lower temperature.[115,116] However, in poor-oxygen atmosphere, there is no enough O_2 to react with Ti^{3+}, hindering the phase transformation.[116]

This assumption was supported by the electron paramagnetic resonance (EPR) analysis of the sample O5, Figure 5.7, where a weak signal was observed at g = 2.013, indicating that most of the Ti^{3+}

species in the sample were oxidized back to the Ti^{4+} ions. Also, this g value is characteristic of the oxygen radical species $O^{\cdot}$ and O^{2-}.[117–119] For TiO_2-CuO composite nanofibers, the diffraction patterns indicated the formation of the anatase phase in air and rutile phase in oxygen. In both atmospheres, copper was oxidized to CuO as indicated by the presence of new peaks at $2\Theta = 35.5°$ and 38.7° corresponding to the -111, 002 (both appear at the 35.5°), and 111, respectively.

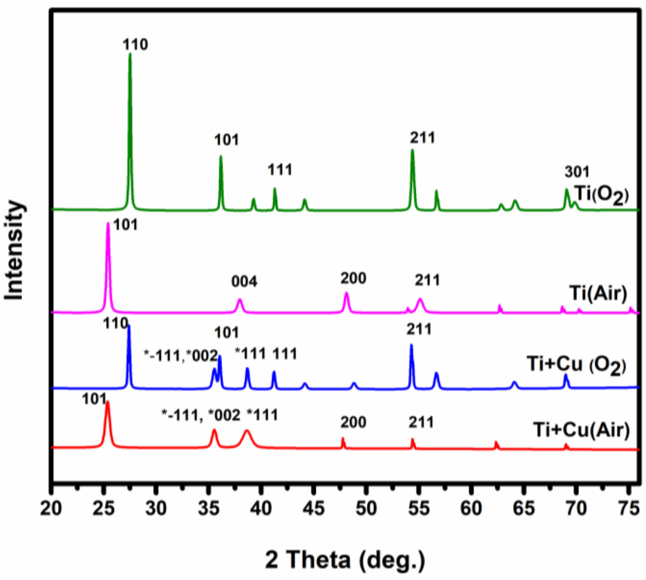

Figure 5.6 XRD pattern of the fabricated nanofibers annealed in different annealing atmospheres.

For the samples annealed in air atmosphere, after the incorporation of CuO with TiO_2, the diffraction peak at 25.4° became broader and its intensity decreased, indicating a reduction in the crystallite size. This was confirmed by calculating the crystallite size for both samples, which were 318.49 Å and 196.13 Å for A1 and A5, respectively. Since Cu^{2+} has larger ionic radius (0.73 Å) than Ti^{4+} (0.64 Å), the incorporated Cu^{2+} ions may distort the lattice structure of TiO_2. This was confirmed by calculating the microstrain, which was found to be 0.551 for A1 and 0.895 for A5. These findings might suggest the creation of substitutional defects by replacing some of the Ti^{4+} ions with Cu^{2+} ions. [120]

The formation of oxygen vacancies in the lattice of TiO_2 is also possible to compensate for the change difference.[120,41]. On the other hand, for the oxygen-annealed samples, the broadening of the peak at 27.4° was the same for both TiO_2 and TiO_2-CuO composite nanofibers samples. This might be attributed to the rutile structure being more compact than the anatase phase, requiring more energy to remove the Ti^{4+} ions from the rutile crystal structure and replace it with Cu^{2+} ions.

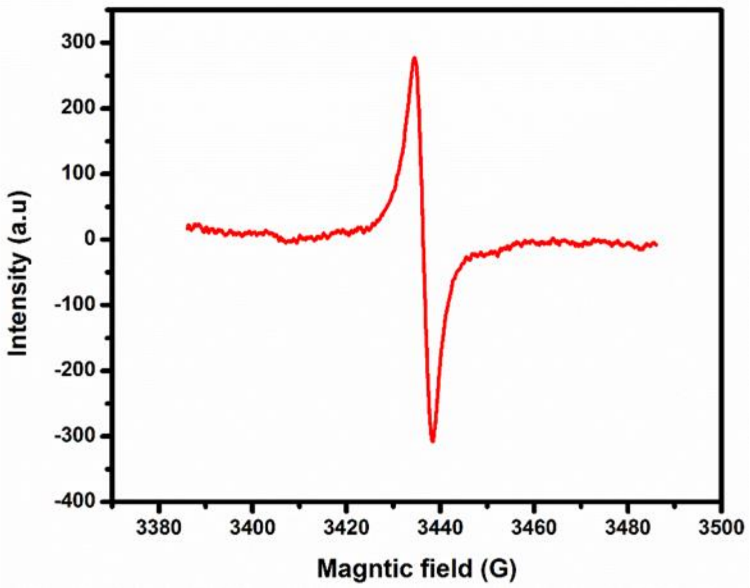

Figure 5.7 EPR spectra of TiO_2-Cu nanofiber annealed in oxygen.

Electron paramagnetic resonance (EPR) analysis was performed for the sample A4 to confirm the presence of Ti^{3+} species, and the coordination of the Cu^{2+} in the frame work of TiO_2, Figure 5.8 The EPR signal is asymmetric, indicating the distortion of the octahedral coordination of TiO_2, possibly due to the replacement of Ti^{4+} ions with Cu^{2+} in the anatase structure. The EPR spectra show an intense peak at g_{II} = 2.00072 and another peak at $g_{\perp}$ = 2.062, indicating that Cu^{2+} substituted Ti^{4+} ions in the octahedral coordination system. As the value of $g_{\perp}$ is larger than that of g_{II}, the ground state of the resulting structure is $^2A_{1g}$.[41,120–122] The observed peak broadening can be attributed to the dipolar interaction between Cu^{2+} ions.[120]

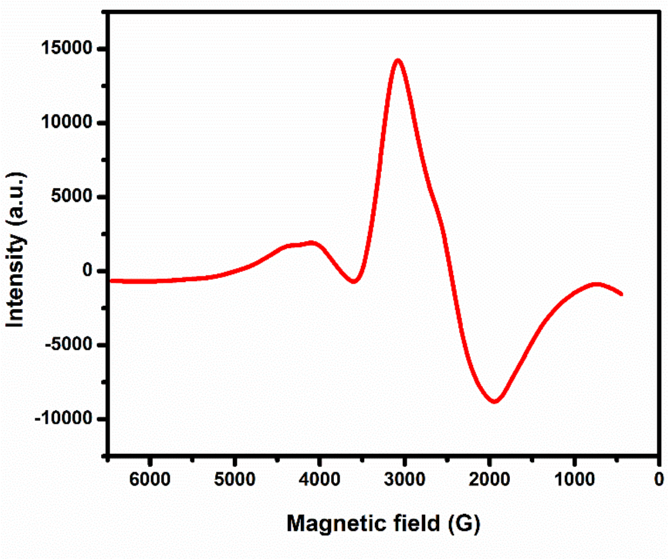

Figure 5.8 EPR spectra of TiO_2-CuO composite nanofiber annealed in air.

Figure 5.9 shows the Raman spectra of the nanofibers annealed in different atmospheres. The TiO_2 nanofibers annealed in air showed the major four Raman bands of anatase at 158, 410, 524, and 646 cm^{-1}, corresponding to E_g, B_{1g}, A_{1g} and E_g active modes, respectively. On the other hand, the TiO_2 nanofibers annealed in oxygen showed the typical Raman bands of rutile at 163, 265, 445, and 618 cm^{-1}, corresponding to the B_{1g}, two phonon scattering, E_g, and A_{1g} modes, respectively.[114] The Raman spectra was almost the same for the Ti-CuO composite nanofibers with a very small shift, even for the samples containing the highest copper concentration.[43,113] A new peak was observed at 276 cm^{-1} that can be assigned to the A_g mode of CuO.[43] The Ti-O bond lengths (R) were calculated using Eq. 1 and was found to be (2 × 1.88, 3 × 2.01 and 2.17 Å) for TiO_2 nanofibers and (2 × 1.9, 3 × 2.15 and 2.4 Å) for TiO_2-CuO composite nanofibers based on the observed Raman bands at 645, 526, and 409 cm^{-1}. These results prevail that the TiO_6 octahedron in anatase was distorted in case of TiO_2-CuO composite nanofibers.[114]

$$\upsilon_{Ti-O} = 722e^{-1.54946(R-1.809)} \qquad (5.1)$$

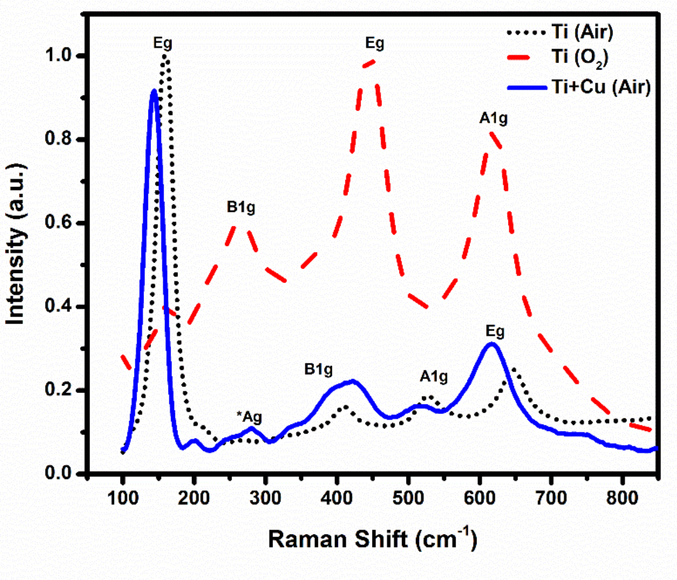

Figure 5.9 Raman shift of the electrospun nanofibers annealed in different atmospheres.

5.4 Optical Properties

Figure 5.10a shows the UV-Vis absorption spectra of the fabricated nanofibers. The TiO_2 samples annealed in air and oxygen atmospheres exhibited an absorption in the UV region of the light spectrum with a peak at 400 nm and 410, respectively. However, a significant red shift in the absorption spectra was observed for the TiO_2-CuO composite nanofibers. As the concentration of CuO increases, the absorption edge extends to a wider range of the light spectrum, with the sample containing the highest CuO concentration show an extended absorption to the near IR region, corresponding to a bandgap energy of 1.4 eV. Figure 5.10b shows the corresponding Tauc plots, plotted using the Eq. 5.2. Note that as the concentration of CuO increases, the optical band gap decreases from 3 eV for TiO_2 nanofibers to 1.45 eV for the sample with the highest copper concentration (A5). This comes in agreement with the study conducted by Chen et al. on the effect of CuO/TiO_2 photocatalyst with different loadings of CuO, where they found that there was a shift in the absorption edge for the CuO/TiO_2 to lower energy as the loading of CuO increased.[36]

$$\alpha h\nu = C(h\nu - E_g)^n \tag{5.2}$$

where *v* is the frequency of photons, (n = 2 for indirect band gap semiconductors), C is a constant, h is the Plank’s constant (6.626 × 10−34J-s), and Eg is the average band-gap energy.

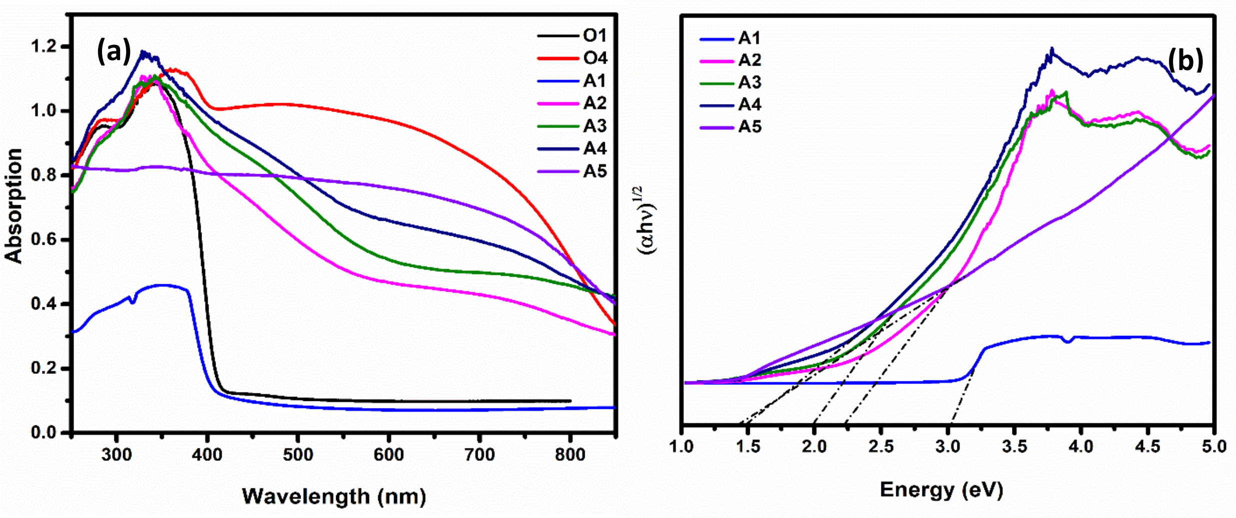

Figure 5.10 UV-Visible absorbance spectra of the TiO_2-CuO composite nanofibers with different copper loadings annealed in (a) oxygen and air atmospheres and (b) the corresponding Tauc plots of the air annealed samples.

5.5 Photocatalytic and Photoelectrochemical Measurements

The photocatalytic H_2 production activity of the fabricated nanofibers was evaluated under irradiation with a 300 W xenon arc lamp using 1M KOH solution, Figure 5.11a, b. For TiO_2 nanofibers, the anatase nanofibers showed the highest H_2 yield (1253 μmol g^{-1}), while the rutile nanofibers resulted in lower H_2 yield (919 μmol g^{-1}) due to its band misalignment with the water redox potentials. For both the oxygen- and air-annealed samples, the incorporation of CuO greatly enhances the amount of hydrogen evolved.

Figure 5.12 shows the normal volcano shape usually seen in catalysis research, where the amount of evolved hydrogen increases with increasing the CuO loading till 0.1 g (1116 and 2715 μmol g^{-1} for the nanofibers annealed in oxygen and air atmospheres, respectively) then declines upon increasing the CuO loading to 0.125 g. This might be attributed to the shielding effect caused by CuO at concentrations higher than 0.1g, as most of the solar radiation would be absorbed by CuO, thus lower amount of the light is able to reach TiO_2 to excite the electrons in the VB.[41,123]

The enhancement in the hydrogen yield can be attributed to the transfer of electrons from the conduction band of TiO_2 to the lower conduction band of CuO,[40,45,124] due to the formation of a p–n junction between TiO_2 and CuO. This p-n junction is very effective in separating the photogenerated charge carriers and hence enhancing the photocatalytic activity. The hydrogen yield obtained from the fabricated TiO_2-CuO composite nanofibers in absence of a hole scavenger in the electrolyte, is superior compared to previous reports.

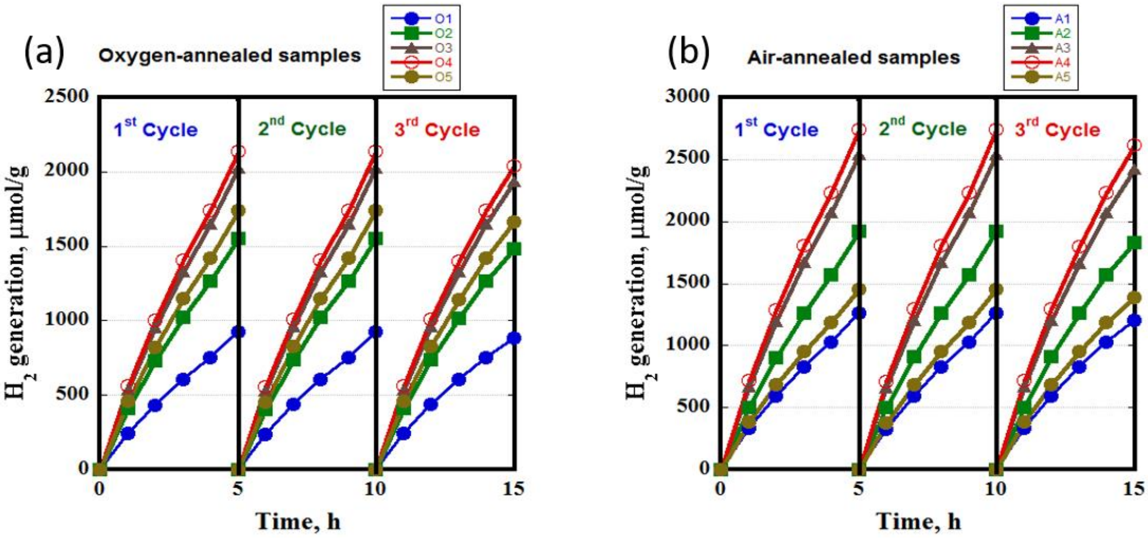

Figure 5.11 H_2 evolution measurements for the oxygen annealed samples (a), the air annealed samples (b), and the correlation between the H_2 evolution of the different annealing atmospheres and different copper loading.

Recently, CuO_x/TiO_2 composite films were tested for photocatalytic water splitting, with reported hydrogen yield of only 50 $mmol.m^{-2}h^{-1}$.[34] Ternary TiO_2/CuO/Cu mesoporous nanofibers were also tested for photocatalytic water splitting, with the highest hydrogen yield obtained of 4000 µmol g^{-1}.[37] However, both studies used hole scavenger in the electrolyte to reduce the recombination rate. In this regard, our obtained hydrogen yield, with no hole scavengers, is considered superior. To test the stability of the fabricated nanofibers, the experiment was repeated for three times. As shown in Figure 5.11a, b, the samples showed high stability along 15 hours, then a slight decrease in the hydrogen yield was observed.

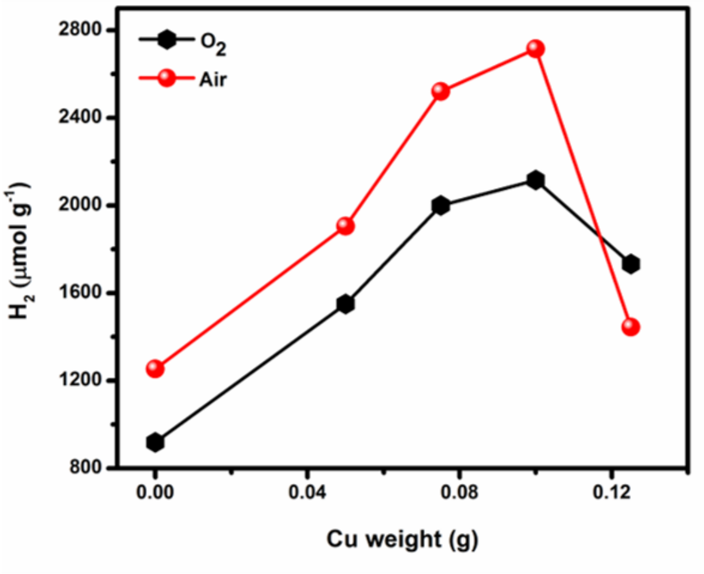

Figure 5.12 The correlation between the H_2 evolution of the different annealing atmospheres and different copper loading.

The photoelectrochemical activity of the fabricated nanofibers to split water was also evaluated, Figure 5.13. The TiO_2-CuO composite nanofibers annealed in air showed superior photocurrent density of almost 0.26 mA cm^{-2} compared to a dark current of 0.05 mA cm^{-2} at 1.0 V_{SCE}. The TiO_2 nanofibers, on the other hand, showed lower photocurrent density of almost 0.2 mA cm^{-2}, and a high dark current of 0.1 mA cm^{-2}. This comes in agreement with the results conducted by Tao et al. for Cu_xO quantum dots deposited on TiO_2 films.[125] However, the overpotential was still relatively high (0.55 V_{SCE}), which was mostly attributed to the resistance due to the discontinuity of the nanofibers layer deposited on the electrode. Nevertheless, these findings indicate the positive effect of CuO when combined with TiO_2 to form a more efficient photocatalyst to split water.

The enhanced behavior can be related to the nature of the created defects upon CuO incorporation. To this end, the defect sensitivity factor (S).[126]

$$S = \frac{c_{dark}}{c_{light}} \qquad (5.2)$$

where c is the current density shift term that can be defined as $c = \frac{J_{gas}}{J_{air}}$, was calculated for the samples A1 and A4.

The sensitivity factor was found to be 0.325, indicating the formation of shallow impurity level by the conduction band of CuO. This can explain the increase in photocurrent density for TiO_2-CuO composite nanofibers compared to that of TiO_2 nanofibers, facilitating the transfer of more electrons to the CB.

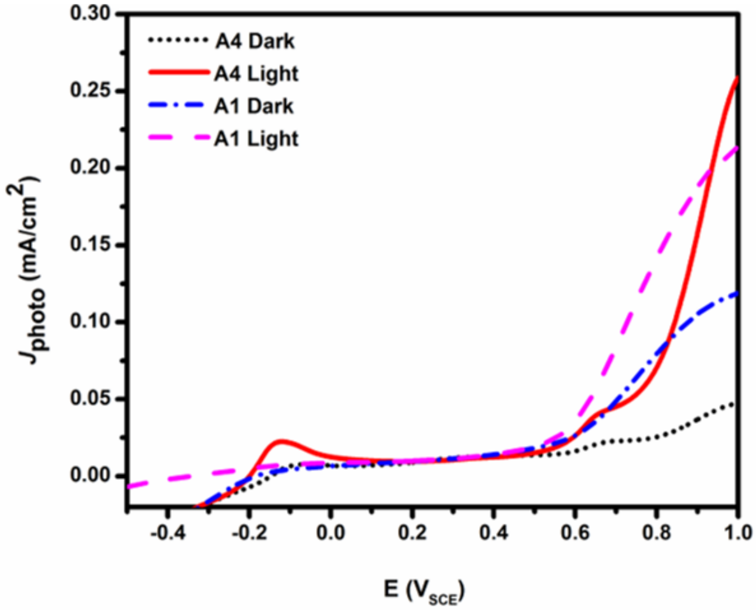

Figure 5.13 Photoelectrochemical measurements of the samples A1 and A4 in dark and under illumination.

5.6 Conclusion

In this study, TiO_2 and TiO_2-CuO composite nanofibers were fabricated and their structural, thermal, optical and photocatalytic properties were compared. Annealing in different atmospheres was found to influence the crystalline phase and thus photocatalytic activity of the fabricated nanofibers. For the nanofibers crystallized in anatase phase, XRD and EPR analysis suggest the substitution of some of the Ti^{4+} ions by Cu^{2+} ions, leading to the formation of shallow defect states below the conduction band of TiO_2. Those shallow defects result in a bandgap narrowing and facilitate charge carriers transport and separation. Besides, as the position of the conduction band of CuO is lower than the conduction band of TiO_2, electrons can easily be transferred to CuO, thus enhancing the charge separation process, leaving free charge carriers needed to perform the redox reaction increases. This was supported by measuring the amount of hydrogen evolved, where TiO_2-CuO showed 117% enhancement compared to TiO_2 nanofibers. The results of this study prove that manipulating the band structure of TiO_2 using optimized composite formation can be a very promising approach to overcome the limitations of TiO_2 as a photocatalyst for water splitting reaction. It also indicates that copper shows an immense potential as a co-catalyst for photocatalytic water splitting and has a remarkable effect in hindering the recombination of the photogenerated charge carriers, thus enhancing the charge transfer process.

Chapter 6

Cu^0 Nanoparticles/TiO_2 Nanofibers for Photocatalytic Water Splitting ‡

6.1 Morphological Features

Figure 6.1 shows FESEM images of the fabricated nanofibers before and after annealing. The as-electrospun TiO_2 nanofibers were smooth as shown in Figure 6.1a. After annealing in argon atmosphere, the structure of the nanofibers was completely different, Figure 6.1b. The change in diameter was hard to detect, due to the incomplete combustion of the polymer (PVP), which is expected when the annealing process is performed in an inert atmosphere. However, nanoparticles imbedded in the fiber were detected, which were further investigated using TEM.

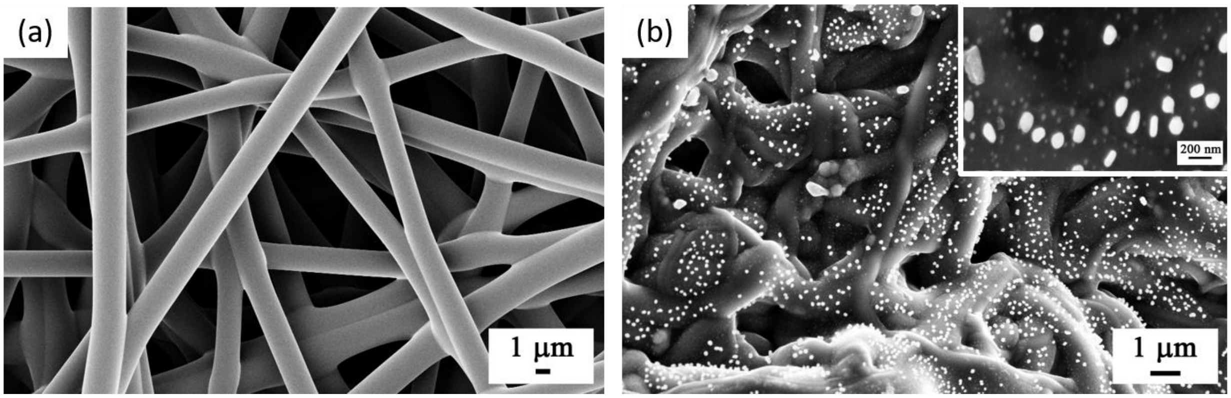

Figure 6.1 FESEM images of the electrospun (a) Titanium-copper nanofibers before annealing, (b) Titanium-copper nanofibers after annealing.

---

‡ This Chapter has been submitted for publication: Menna M. Hasan and Nageh K. Allam, In-situ Formation of Copper Nanoparticles Impeded in TiO_2 Nanofibers Significantly Enhances the Efficiency of Photocatalytic Water Splitting.

6.2 Optical Properties

The UV-Vis spectrum, Figure 6.2, showed high absorption intensity and a shift towards the visible region of the solar spectrum (almost 800 nm) for both TiO_2 and TiO_2-Cu composite nanofiber, which is consistent with the black color observed for both samples. This shift can be related to the formation of graphene in the samples during annealing, which is in agreement with previous studies.[127] On the other hand, a recent study by Samani et al. who fabricated black titania core-shell nanoparticles by annealing the synthesized nanoparticles in argon atmosphere at different temperatures, the shift in the absorption spectrum was attributed to the formation of thin Ti_2O_3 surface layer.[128] Li et al. measured the absorbance of carbon-doped TiO_2 and noticed that there was a shift in the absorption up to 700 nm, which enhanced the photocatalytic activity compared to TiO_2 nanofibers. They suggested that this shift is due to the formation of Ti^{3+} defect states between the conduction band and the valence band of TiO_2.[129]

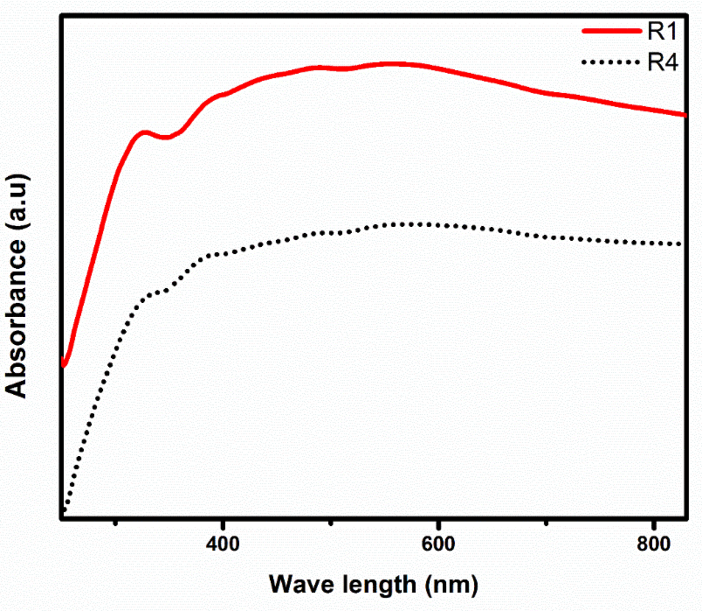

Figure 6.2 UV-Visible absorbance spectra of TiO_2 nanofibers R1, and TiO_2-Cu composite nanofibers R4.

6.3 Structural and Elemental Analysis

As shown in Figure 6.3, XRD analysis was performed to study the effect of annealing at different temperatures in argon atmosphere on phase transformations, and whether copper facilitates or inhibits the phase transformation from anatase to rutile. For titanium nanofibers annealed at 500 °C, a characteristic peak of the (101) facet of the anatase phase was observed at 25.4°. However, titanium nanofibers annealed at 600 °C showed two peaks at 25.4° and 27.17° corresponding to (101) of the anatase phase and (110) of the rutile phase. This comes in agreement with the results obtained from a recent study, where a mixture of anatase and rutile phases was obtained when TiH_2 powder was annealed in argon atmosphere at 530 °C.[130] Eq 6.1 was used to determine the rutile percentage in the nanofibers.[131]

$$\text{Rutile percentage\%} = [1/ (1 + 0.79I_A/I_R)] * 100 \qquad (6.1)$$

where I_R and I_A are the peak intensities of (110) and (101) reflections for rutile and anatase, respectively.[132] It was found that the anatase-to-rutile ratio is 60:40 respectively. For Ti-Cu composite nanofibers (R2) annealed at 600 °C, we noticed the presence of new peaks at $2\Theta = 43.3°, 50.4°, 74.2°$, which correspond to the (111), (200), and (220) facets of face-centered cubic copper, respectively,[70,133,134] besides the sharp peak at 25.2° corresponding to the anatase phase. While no peak related to the rutile phase was detected, indicating that copper stabilizes the anatase phase and hinders the transformation to rutile phase. For Ti-Cu composites with higher copper loadings (R3, R4, and R5), we were not able to detect the peaks related to TiO_2, due to the high intensity of the peaks related to copper. However, for the sample with the highest copper loading (R5), a new peak related to graphene was detected at $2\Theta = 24°$. According to previous studies the low intensity of this peak is due to the low crystallinity of this graphene and the high intensity of the copper peaks.[133]

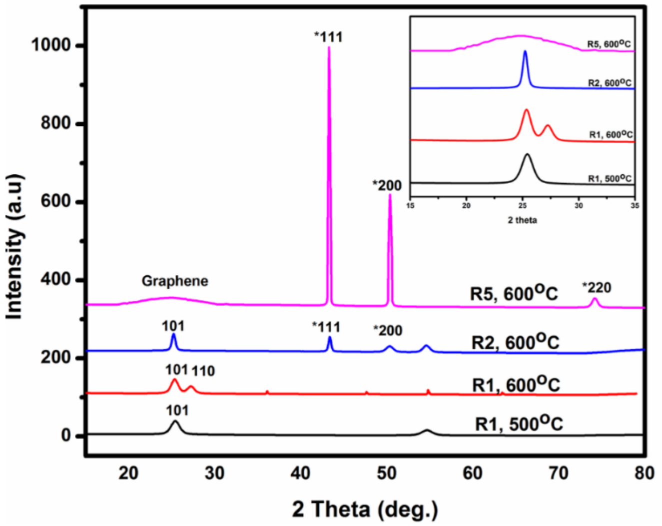

Figure 6.3 XRD pattern of the fabricated nanofibers annealed at different temperatures.

The obtained Raman spectra for TiO_2 nanofibers showed the major four Raman bands of anatase at 158, 410, 524, and 646 cm^{-1}, which correspond to Eg, B1g, A1g and Eg active modes, respectively, as shown in Figure 6.4a. For the TiO_2-Cu composite, the typical peaks of the D and G bands were observed at 1360 cm^{-1} and 1590 cm^{-1}.[91,94,135–138] The D band is attributed to the local defects, while the G band is related to sp^2 hybridized graphene domains.[139] As shown in Figure 6.4b,there was a an increase in the intensity of the peaks related to the D and G bands for the composites R4 and R5 compared to that of TiO_2 nanofibers. There was a significant increase in the intensity of the D and G bands for the composites R2 and R3, indicating an optimum ratio of copper to PVP that facilitates the formation of graphene. This might be due to the consumption of larger amount of carbon in maintaining the excess amount of copper at zero-valent state. This is supported by the results obtained from XRD measurements, Figure 6.3, where, the intensity of the peaks related to metallic copper is much stronger than that of graphene. This comes in agreement with the results conducted recently, where lignin was used as a carbon source, it was found that the amount of graphene formed was dependent on the amount of copper present in the sample.[133]

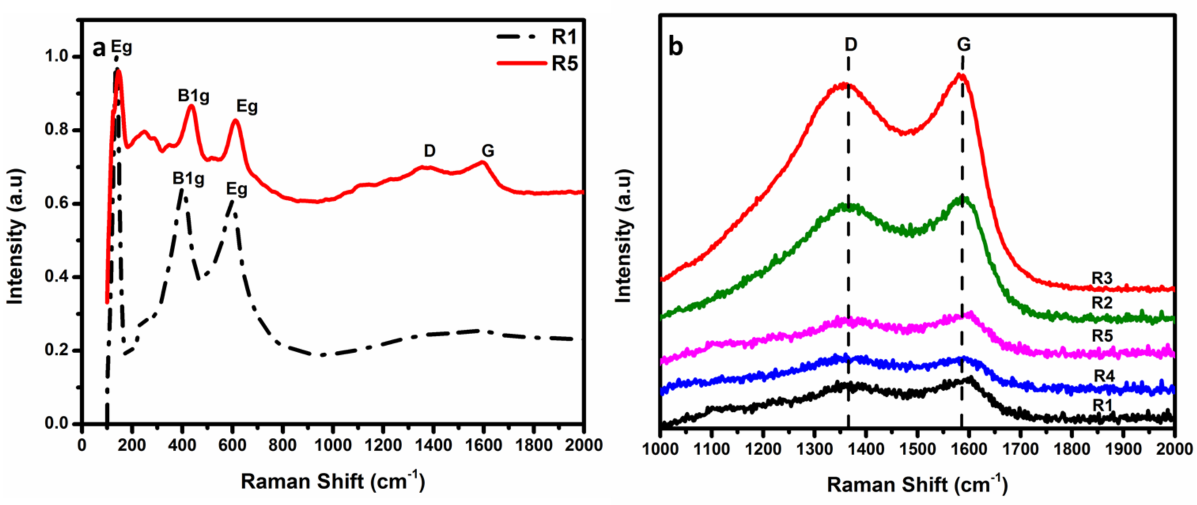

Figure 6.4 (a) Raman shift of TiO_2 nanofibers R1, and TiO_2-Cu composite nanofibers R4 (b) The change in D and G bands intensity with copper loadings.

FTIR analysis was performed to study the composition of the fabricated nanofibers. As shown in Figure 6.5, the band at 594 cm^{-1} is characteristic of the Ti-O-Ti bond,[140] another peak was observed at 3419 cm^{-1}, which corresponds to the stretching vibration of the hydroxyl groups OH^- group.[91,140–142] While the band at 1300 cm^{-1} is related to C-N.[91,143] The peak at 1700 cm^{-1} is related to C=O. The broad bands at 1400 and 1230 cm^{-1} are assigned to the deformation of O–H vibration from C–O and C–OH stretching vibrations in C–OH.[143] The peak at 850 cm^{-1} is characteristic of the epoxide groups,[139,144] and the peak at 1560 cm^{-1} is related to the skeletal vibration of graphene sheets.[139,145]

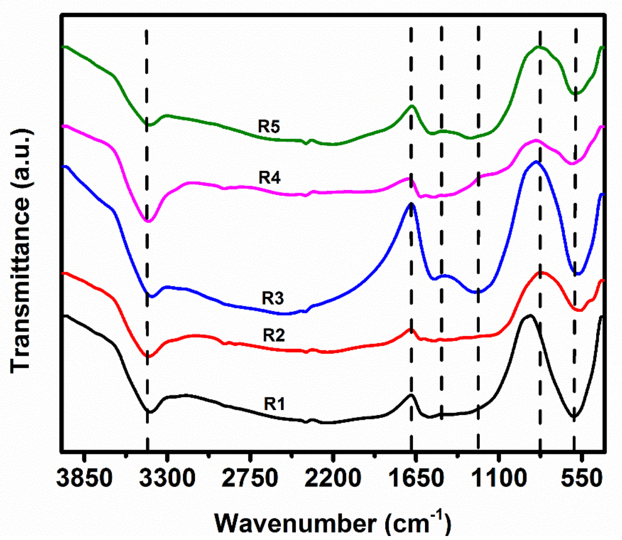

Figure 6.5 FTIR spectra of the fabricated nanofibers with different copper loadings.

The data obtained from electron paramagnetic resonance (EPR) measurements, Figure 6.6, showed a peak at g = 2.008, which indicates the presence of carbon centered radicals due to the incomplete oxidation of the PVP polymer.[130] For the TiO_2-Cu composite, the intensity of the peak was very weak, which can be related to larger amount of the polymer undergoing an oxidative reaction through electron transfer to copper atoms. This also explains the stabilization of copper metal at zero oxidation state.

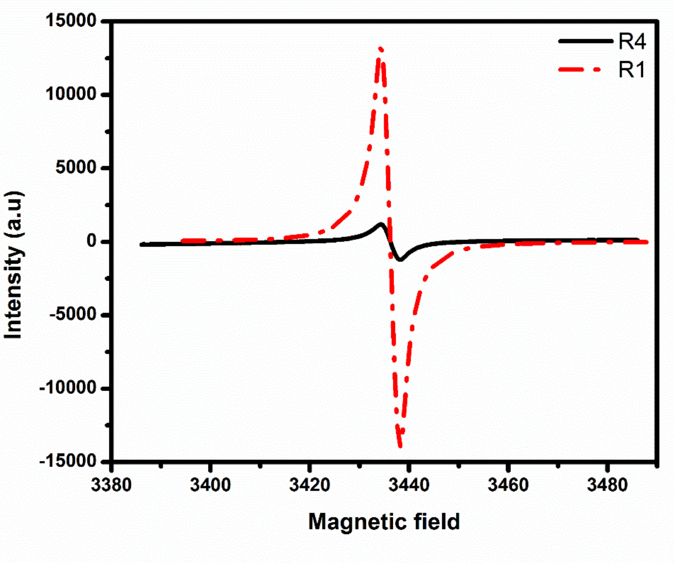

Figure 6.6 EPR spectra of TiO_2 nanofibers R1, and TiO_2-Cu composite nanofibers R4.

As shown in Figure 6.7a, the measured vertical d-spacing of the lattice is 3.52 A° and 2.1 A° which correspond to the (101) lattice planes of the anatase phase of TiO_2,[146] and the (111) lattice plane of metallic copper, as shown in Figure 6.7b.[147] The particle size of copper nanoparticles was found to be in the range of 23 - 33 nm, which are well distributed among the nanofibers, as shown in Figure 6.7c. Moreover, the electron diffraction patterns shown in Figure 6.7d, confirm that the material is polycrystalline.

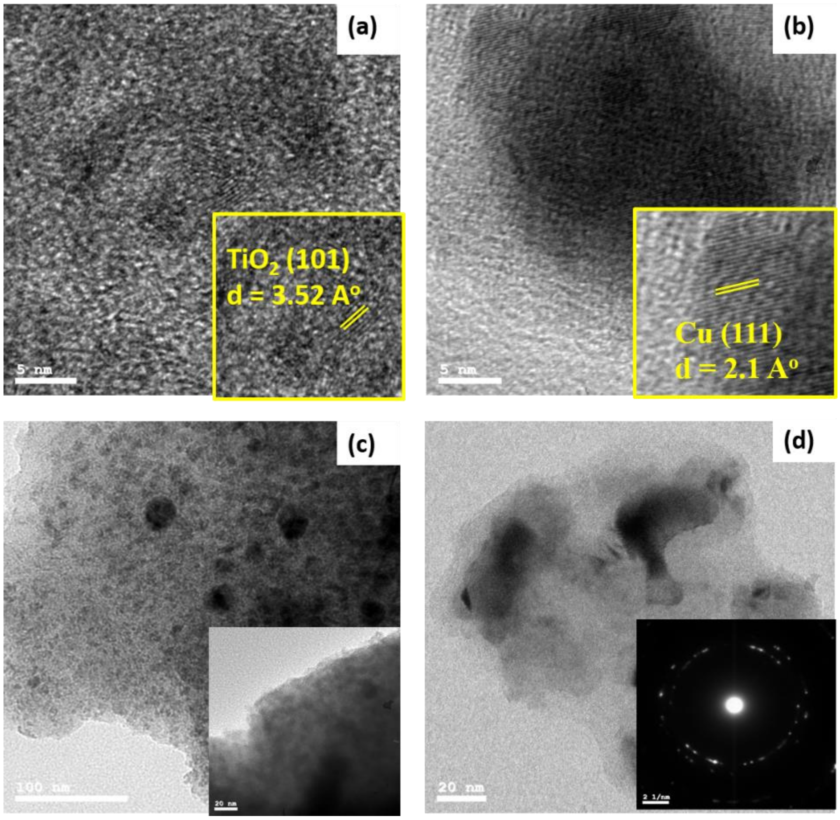

Figure 6.7 TEM images of TiO_2-Cu composite nanofibers.

6.4 Photocatalytic Water Splitting Measurements

The photocatalytic activity of the fabricated nanofibers was tested under irradiation with a 300 W xenon arc lamp using a solution of 1M KOH. Figure 6.8 shows the amount of H_2 obtained upon testing the fabricated nanofibers. For TiO_2 nanofibers, the H_2 yield was almost 1150 µmol g^{-1}. The amount of hydrogen collected increased with the increase in copper concentration and reaches the highest H_2 yield of 5110 μmol g^{-1} for the sample containing the highest copper concentration. This could be due to the plasmonic behavior of copper nanoparticles, which results in an increase in the density of the generated charge carriers, along with the enhanced charge separation due to the heterojunction formed at the interface between copper and TiO_2. These values were obtained in absence of hole scavenger species in the electrolyte, making the fabricated TiO_2-Cu composite nanofibers superior in performance compared to the results reported in previous studies. Recently, the catalytic activity of TiO_2 nanotube arrays decorated with Cu nanoparticles only showed 15 μmol cm^{-2}.[148]

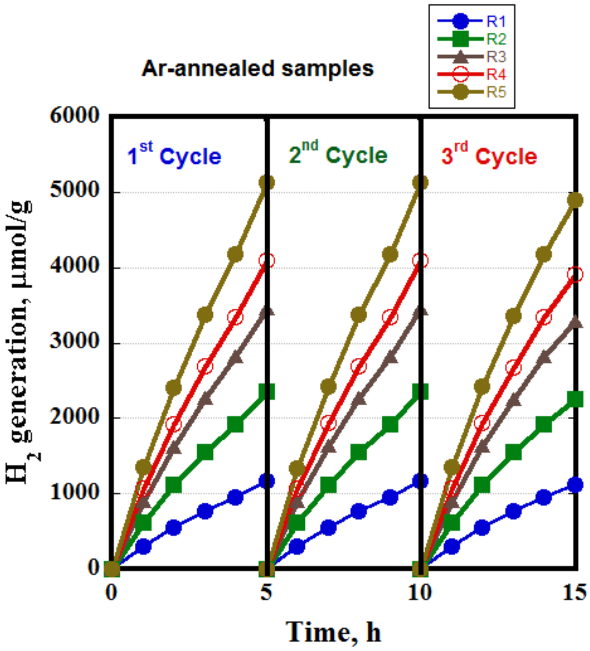

Figure 6.8 H_2 evolution measurements.

6.5 Conclusion

In this study, TiO_2 and TiO_2-Cu composite nanofibers were fabricated, their morphological, structural, optical and photocatalytic properties were studied. Annealing at different temperatures was found to affect the crystallinity of the fabricated materials. The photocatalytic activity of the fabricated nanofibers in water splitting reaction was also tested. Metallic copper nanoparticles were stabilized by the carbon present in the fiber. Copper nanoparticles were found to stabilize the anatase phase. Annealing in argon atmosphere also facilitates the conversion of PVP to graphene. The presence of graphene shifted the absorption to almost 800 nm. For Ti-Cu nanofibers, there was a 344% increase in the hydrogen yield compared to that of TiO_2 nanofibers. This enhancement is attributed to the efficient charge separation due to the presence of copper and graphene. Besides the plasmonic effect of copper nanoparticles increases the number of the generated charge carriers. This study introduces a new approach for stabilizing metallic copper nanoparticles. This study proves that further optimization of composite nanofibers can greatly enhance the efficiency of TiO_2 as a photocatalyst for water splitting reaction and overcome its limitations.

Chapter 7

Summary and Suggestions for Future Work

7.1 Summary

In this Thesis, TiO_2 and TiO_2-Copper composite nanofibers were fabricated and annealed in different atmospheres, oxygen, air, and argon. The effect of different annealing atmospheres on the fabricated composite was studied. In terms of, the change in morphology before and after annealing, the resulting crystal structural, the optical and photocatalytic properties. It was found that annealing in air atmosphere resulted in the formation of anatase phase and CuO, rutile phase and CuO was formed in oxygen atmosphere. While for the argon annealed samples, a mixture of anatase and rutile phases was formed at 500 ^{o}C, at 600 ^{o}C only rutile phase was obtained. However, it was found that copper stabilizes the anatase phase even at 600 ^{o}C. For the anatase phase, XRD and EPR analysis suggest that some of the Ti^{4+} ions were substituted by Cu^{2+} ions, this lead to the formation of shallow defect states below the conduction band of TiO_2. Accordingly, the bandgap became narrower and charge carriers transport and collection was enhanced. Besides, electrons can easily move to the conduction band of CuO due to the lower position of the conduction band relative to that of TiO_2. Thus, charge recombination is hindered. This enhancement in the hydrogen yield also confirms these findings, where TiO_2-CuO of the air annealed samples showed 117% enhancement compared to TiO_2 nanofibers. For the samples annealed in argon atmosphere, metallic copper nanoparticles were stabilized by the carbon present in the fiber. Annealing in argon atmosphere also resulted in converting PVP to graphene. The presence of graphene shifted the absorption to almost 800 nm. This resulted in a percent increase in the hydrogen yield by almost 344% for Ti-Cu nanofibers compared to that of TiO_2 nanofibers. This enhancement is attributed to the efficient charge separation facilitated by the presence of copper and graphene. Besides the plasmonic effect of metallic copper nanoparticles, which increases the number of the generated charge carriers. This study introduces a new approach for metallic copper nanoparticles stabilization, and graphene synthesis. This study prove that further optimization of composite nanofibers can greatly enhance the efficiency of TiO_2 as a photocatalyst for water splitting reaction and overcome its limitations.

7.2 Nanofibers

The structure of the nanofibers is very promising for photocatalysis applications, due to their large surface area and directional charge transfer of the photogenerated charge carriers, hence reduces the recombination rate. Thus, nanofibers of other metals and metal oxides need to be explored and studied for comparison, and to increase the obtained hydrogen yield.

7.3 Metallic Copper Stabilization

The work presented in this thesis shows a great potential of metallic copper in catalysis, thus further investigation need to be conducted on stabilizing copper in zero oxidation state. In this regard, carbon-based materials seem to be very promising in metallic copper stabilization. Thus, other carbon sources can be explored to maintain the zero-valent copper nanostructures.

7.4 Plasmonic Behavior of Metallic Copper Nanoparticles

Plasmonic materials show some unique properties that can be used to enhance the efficiency of the overall photocatalytic water splitting reaction. In this regard, copper nanoparticles show great potential as a plasmonic material with the advantage of being cheap and earth abundant, rather than the conventional plasmonic materials. Such as, gold and silver, which are very expensive and very rare in the earth crust.

7.5 New Approach for Graphene Synthesis

According to the results obtained in this thesis, the polymeric materials used in the electrospinning process can be used as a carbon source and be converted into graphene if the annealing process is conducted in an inert atmosphere. This approach should be further investigated through using catalysts that can accelerate this transformation. Modifying the annealing conditions can also help enhancing the crystal structure of the formed graphene sheets.

REFERENCES

(1) de Oliveira, M. C. K.; Teixeira, A.; Vieira, L. C.; de Carvalho, R. M.; de Carvalho, A. B. M.; do Couto, B. C. Flow Assurance Study for Waxy Crude Oils. *Energy & Fuels* **2012**, *26* (5), 2688–2695.

(2) The International Energy Agency (2011) World energy outlook 2011 https://www.iea.org/publications/freepublications/publication/WEO2011_WEB.pdf (accessed Apr 14, 2018).

(3) Thavasi, V.; Singh, G.; Ramakrishna, S. Electrospun Nanofibers in Energy and Environmental Applications. *Energy Environ. Sci.* **2008**, *1* (2), 205.

(4) Serrano, E.; Rus, G.; García-Martínez, J. Nanotechnology for Sustainable Energy. *Renew. Sustain. Energy Rev.* **2009**, *13* (9), 2373–2384.

(5) Painter, P.; Williams, P.; Mannebach, E. Recovery of Bitumen from Oil or Tar Sands Using Ionic Liquids. *Energy & Fuels* **2010**, *24* (2), 1094–1098.

(6) Lee, M.; Bae, J.; Lee, J.; Lee, C.-S.; Hong, S.; Wang, Z. L. Self-Powered Environmental Sensor System Driven by Nanogenerators. *Energy Environ. Sci.* **2011**, *4* (9), 3359.

(7) Tee, S. Y.; Win, K. Y.; Teo, W. S.; Koh, L. D.; Liu, S.; Teng, C. P.; Han, M. Y. Recent Progress in Energy-Driven Water Splitting. *Adv. Sci.* **2017**, *4* (5).

(8) Grimes, C. A.; Varghese, O. K.; Ranjan, S. *Light, Water, Hydrogen: The Solar Generation of Hydrogen by Water Photoelectrolysis*; Springerlink: Online Service, 2008.

(9) Byrne, J. A.; Dunlop, P. S. M.; Hamilton, J. W. J.; Fernández-Ibáñez, P.; Polo-López, I.; Sharma, P. K.; Vennard, A. S. M. A Review of Heterogeneous Photocatalysis for Water and Surface Disinfection. *Molecules* **2015**, *20* (4), 5574–5615.

(10) Maeda, K.; Domen, K. New Non-Oxide Photocatalysts Designed for Overall Water Splitting under Visible Light. *J. Phys. Chem. C* **2007**, *111* (22), 7851–7861.

(11) Dong, Z.; Kennedy, S. J.; Wu, Y. Electrospinning Materials for Energy-Related Applications and Devices. *J. Power Sources* **2011**, *196* (11), 4886–4904.

(12) Pietrosemoli, L.; Rodríguez Monroy, C. The Impact of Sustainable Construction and Knowledge Management on Sustainability Goals. A Review of the Venezuelan Renewable Energy Sector. *Renew. Sustain. Energy Rev.* **2013**, *27*, 683–691.

(13) Mascal, M.; Nikitin, E. B. Direct, High-Yield Conversion of Cellulose into Biofuel. *Angew. Chemie Int. Ed.* **2008**, *47* (41), 7924–7926.

(14) Bhardwaj, N.; Kundu, S. C. Electrospinning: A Fascinating Fiber Fabrication Technique. *Biotechnol. Adv.* **2010**, *28* (3), 325–347.

(15) Maheswari, D.; Sreenivasan, D. Review of TiO_2 Nanowires in Dye Sensitized Solar Cell. *Appl. Sol. Energy* **2015**, *51* (2), 112–116.

(16) Indira, K.; Mudali, U. K.; Nishimura, T.; Rajendran, N. A Review on TiO_2 Nanotubes: Influence of Anodization Parameters, Formation Mechanism, Properties, Corrosion Behavior, and Biomedical Applications. *J. Bio- Tribo-Corrosion* **2015**, *1* (4), 28.

(17) Lockwood, D. J.; Bin Ding, J. yu. *Electrospun Nanofi Bers for Energy and Environmental Applications*; 2015.

(18) Greiner, A.; Wendorff, J. H. Electrospinning: A Fascinating Method for the Preparation of Ultrathin Fibers. *Angew. Chemie Int. Ed.* **2007**, *46* (30), 5670–5703.

(19) Grimes, C. A.; Mor, G. K. *TiO_2 Nanotube Arrays*; Springer US: Boston, MA, 2009.

(20) Kudo, A.; Miseki, Y. Heterogeneous Photocatalyst Materials for Water Splitting. *Chem. Soc. Rev.* **2009**, *38* (1), 253–278.

(21) Kudo, A.; Miseki, Y. Heterogeneous Photocatalyst Materials for Water Splitting. *Chem. Soc. Rev.* **2009**, *38* (1), 253–278.

(22) Hagfeldt, A.; Graetzel, M. Light-Induced Redox Reactions in Nanocrystalline Systems. *Chem. Rev.* **1995**, *95* (1), 49–68.

(23) Settanni, G.; Zhou, J.; Suo, T.; Schöttler, S.; Landfester, K.; Schmid, F.; Mailänder, V. Protein Corona Composition of PEGylated Nanoparticles Correlates Strongly with Amino Acid Composition of Protein Surface. **2016**.

(24) Ge, M.; Cao, C.; Huang, J.; Li, S.; Chen, Z.; Zhang, K.-Q.; Al-Deyab, S. S.; Lai, Y. A Review of One-Dimensional TiO_2 Nanostructured Materials for Environmental and Energy Applications. *J. Mater. Chem. A* **2016**, *4* (18), 6772–6801.

(25) Haggerty, J. E. S.; Schelhas, L. T.; Kitchaev, D. A.; Mangum, J. S.; Garten, L. M.; Sun, W.; Stone, K. H.; Perkins, J. D.; Toney, M. F.; Ceder, G.; et al. High-Fraction Brookite Films from Amorphous Precursors. *Sci. Rep.* **2017**, *7* (1), 15232.

(26) Pelaez, M.; Nolan, N. T.; Pillai, S. C.; Seery, M. K.; Falaras, P.; Kontos, A. G.; Dunlop, P. S. M.; Hamilton, J. W. J.; Byrne, J. A.; O’Shea, K.; et al. A Review on the Visible Light Active Titanium Dioxide Photocatalysts for Environmental Applications. *Appl. Catal. B Environ.* **2012**, *125*, 331–349.

(27) Choi, W.; Termin, A.; Hoffmann, M. R. The Role of Metal Ion Dopants in Quantum-Sized TiO_2: Correlation between Photoreactivity and Charge Carrier Recombination Dynamics. *J. Phys. Chem.* **1994**, *98* (51), 13669–13679.

(28) Herrmann, J.-M. Heterogeneous Photocatalysis: State of the Art and Present Applications In Honor of Pr. R.L. Burwell Jr. (1912–2003), Former Head of Ipatieff Laboratories, Northwestern University, Evanston (Ill). *Top. Catal.* **2005**, *34* (1–4), 49–65.

(29) Engweiler, J.; Harf, J.; Baiker, A. WO_x/TiO_2 Catalysts Prepared by Grafting of Tungsten Alkoxides: Morphological Properties and Catalytic Behavior in the Selective Reduction of NO by NH3. *J. Catal.* **1996**, *159* (2), 259–269.

(30) Vinodgopal, K.; Kamat, P. V. Enhanced Rates of Photocatalytic Degradation of an Azo Dye Using SnO_2/TiO_2 Coupled Semiconductor Thin Films. *Environ. Sci. Technol.* **1995**, *29* (3), 841–845.

(31) Ohtani, B.; Kakimoto, M.; Nishimoto, S.; Kagiya, T. Photocatalytic Reaction of Neat Alcohols by

Metal-Loaded Titanium(IV) Oxide Particles. *J. Photochem. Photobiol. A Chem.* **1993**, *70* (3), 265–272.

(32) Sclafani, A.; Herrmann, J.-M. Influence of Metallic Silver and of Platinum-Silver Bimetallic Deposits on the Photocatalytic Activity of Titania (Anatase and Rutile) in Organic and Aqueous Media. *J. Photochem. Photobiol. A Chem.* **1998**, *113* (2), 181–188.

(33) Yu, J. C.; Yu; Ho; Jiang; Zhang. Effects of F - Doping on the Photocatalytic Activity and Microstructures of Nanocrystalline TiO_2 Powders. *Chem. Mater.* **2002**, *14* (9), 3808–3816.

(34) Hu, Q.; Huang, J.; Li, G.; Chen, J.; Zhang, Z.; Deng, Z.; Jiang, Y.; Guo, W.; Cao, Y. Effective Water Splitting Using CuOx/TiO_2 Composite Films: Role of Cu Species and Content in Hydrogen Generation. *Appl. Surf. Sci.* **2016**, *369*, 201–206.

(35) Zhu, L.; Hong, M.; Ho, G. W. Fabrication of Wheat Grain Textured TiO_2/CuO Composite Nanofibers for Enhanced Solar H_2 Generation and Degradation Performance. *Nano Energy* **2015**, *11*, 28–37.

(36) Chen, W. T.; Jovic, V.; Sun-Waterhouse, D.; Idriss, H.; Waterhouse, G. I. N. The Role of CuO in Promoting Photocatalytic Hydrogen Production over TiO_2. *Int. J. Hydrogen Energy* **2013**, *38* (35), 15036–15048.

(37) Hou, H.; Shang, M.; Gao, F.; Wang, L.; Liu, Q.; Zheng, J.; Yang, Z.; Yang, W. Highly Efficient Photocatalytic Hydrogen Evolution in Ternary Hybrid TiO_2/CuO/Cu Thoroughly Mesoporous Nanofibers. *ACS Appl. Mater. Interfaces* **2016**, *8* (31), 20128–20137.

(38) Xu, S.; Du, A. J.; Liu, J.; Ng, J.; Sun, D. D. Highly Efficient CuO Incorporated TiO2 Nanotube Photocatalyst for Hydrogen Production from Water. *Int. J. Hydrogen Energy* **2011**, *36* (11), 6560–6568.

(39) Bandara, J.; Udawatta, C. P. K.; Rajapakse, C. S. K. Highly Stable CuO Incorporated TiO_2 Catalyst for Photocatalytic Hydrogen Production from H_2O. *Photochem. Photobiol. Sci.* **2005**, *4* (11), 857.

(40) Lei, M.; Wang, N.; Zhu, L.; Zhou, Q.; Nie, G.; Tang, H. Photocatalytic Reductive Degradation of

Polybrominated Diphenyl Ethers on CuO/TiO_2 nanocomposites: A Mechanism Based on the Switching of Photocatalytic Reduction Potential Being Controlled by the Valence State of Copper. *Appl. Catal. B Environ.* **2016**, *182*, 414–423.

(41) Li, G.; Dimitrijevic, N. M.; Chen, L.; Rajh, T.; Gray, K. a. Role of Surface/Interfacial Cu^{2+} Sites in the Photocatalytic Activity of Coupled CuO−TiO_2 Nanocomposites. *J. Phys. Chem. C* **2008**, *112* (48), 19040–19044.

(42) Ganesh, I.; Kumar, P. P.; Annapoorna, I.; Sumliner, J. M.; Ramakrishna, M.; Hebalkar, N. Y.; Padmanabham, G.; Sundararajan, G. Preparation and Characterization of Cu-Doped TiO_2 Materials for Electrochemical, Photoelectrochemical, and Photocatalytic Applications. *Appl. Surf. Sci.* **2014**, *293*, 229–247.

(43) Pai, M. R.; Banerjee, A. M.; Rawool, S. A.; Singhal, A.; Nayak, C.; Ehrman, S. H.; Tripathi, A. K.; Bharadwaj, S. R. A Comprehensive Study on Sunlight Driven Photocatalytic Hydrogen Generation Using Low Cost Nanocrystalline Cu-Ti Oxides. *Sol. Energy Mater. Sol. Cells* **2016**, *154*, 104–120.

(44) Marschall, R. Semiconductor Composites: Strategies for Enhancing Charge Carrier Separation to Improve Photocatalytic Activity. *Adv. Funct. Mater.* **2014**, *24* (17), 2421–2440.

(45) Moniz, S. J. A.; Tang, J. Charge Transfer and Photocatalytic Activity in CuO/TiO_2 Nanoparticle Heterojunctions Synthesised through a Rapid, One-Pot, Microwave Solvothermal Route. *ChemCatChem* **2015**, *7* (11), 1659–1667.

(46) Janczarek, M.; Kowalska, E. On the Origin of Enhanced Photocatalytic Activity of Copper-Modified Titania in the Oxidative Reaction Systems. *Catalysts* **2017**, *7* (11), 317.

(47) Ueno, K.; Misawa, H. Surface Plasmon-Enhanced Photochemical Reactions. *J. Photochem. Photobiol. C Photochem. Rev.* **2013**, *15*, 31–52.

(48) Kowalska, E.; Mahaney, O. O. P.; Abe, R.; Ohtani, B. Visible-Light-Induced Photocatalysis through Surface Plasmon Excitation of Gold on Titania Surfaces. *Phys. Chem. Chem. Phys.* **2010**, *12* (10), 2344.

(49) Ingram, D. B.; Linic, S. Water Splitting on Composite Plasmonic-Metal/Semiconductor Photoelectrodes: Evidence for Selective Plasmon-Induced Formation of Charge Carriers near the Semiconductor Surface. *J. Am. Chem. Soc.* **2011**, *133* (14), 5202–5205.

(50) Yamaguchi, T.; Kazuma, E.; Sakai, N.; Tatsuma, T. Photoelectrochemical Responses from Polymer-Coated Plasmonic Copper Nanoparticles on TiO_2. *Chem. Lett.* **2012**, *41* (10), 1340–1342.

(51) Zhang, S.; Peng, B.; Yang, S.; Wang, H.; Yu, H.; Fang, Y.; Peng, F. Non-Noble Metal Copper Nanoparticles-Decorated TiO_2 Nanotube Arrays with Plasmon-Enhanced Photocatalytic Hydrogen Evolution under Visible Light. *Int. J. Hydrogen Energy* **2015**, *40* (1), 303–310.

(52) DeSario, P. A.; Pietron, J. J.; Brintlinger, T. H.; McEntee, M.; Parker, J. F.; Baturina, O.; Stroud, R. M.; Rolison, D. R. Oxidation-Stable Plasmonic Copper Nanoparticles in Photocatalytic TiO_2 Nanoarchitectures. *Nanoscale* **2017**, *9* (32), 11720–11729.

(53) Yan, J.; Wu, G.; Guan, N.; Li, L. Synergetic Promotion of the Photocatalytic Activity of TiO_2 by Gold Deposition under UV-Visible Light Irradiation. *Chem. Commun.* **2013**, *49* (100), 11767.

(54) Kaur, R.; Pal, B. Plasmonic Coinage Metal–TiO_2 Hybrid Nanocatalysts for Highly Efficient Photocatalytic Oxidation under Sunlight Irradiation. *New J. Chem.* **2015**, *39* (8), 5966–5976.

(55) Singh, M.; Sinha, I.; Premkumar, M.; Singh, A. K.; Mandal, R. K. Structural and Surface Plasmon Behavior of Cu Nanoparticles Using Different Stabilizers. *Colloids Surfaces A Physicochem. Eng. Asp.* **2010**, *359* (1–3), 88–94.

(56) Pastoriza-Santos, I.; Sánchez-Iglesias, A.; Rodríguez-González, B.; Liz-Marzán, L. M. Aerobic Synthesis of Cu Nanoplates with Intense Plasmon Resonances. *Small* **2009**, *5* (4), 440–443.

(57) Kanninen, P.; Johans, C.; Merta, J.; Kontturi, K. Influence of Ligand Structure on the Stability and Oxidation of Copper Nanoparticles. *J. Colloid Interface Sci.* **2008**, *318* (1), 88–95.

(58) Chen, D.; Feng, H.; Li, J. Graphene Oxide: Preparation, Functionalization, and Electrochemical Applications. *Chem. Rev.* **2012**, *112* (11), 6027–6053.

(59) Li, D.; Kaner, R. B. Graphene-Based Materials. *Science (80-.).* **2008**, *320* (5880), 1170–1171.

(60) Sykes, E. C. H. Graphene Goes Undercover. *Nat. Chem.* **2009**, *1* (3), 175–176.

(61) Brumfiel, G. Graphene Gets Ready for the Big Time. *Nature* **2009**, *458* (7237), 390–391.

(62) Geim, A. K.; Novoselov, K. S. The Rise of Graphene. *Nat. Mater.* **2007**, *6* (3), 183–191.

(63) Park, S.; Ruoff, R. S. Chemical Methods for the Production of Graphenes. *Nat. Nanotechnol.* **2009**, *4* (4), 217–224.

(64) Stoller, M. D.; Park, S.; Zhu, Y.; An, J.; Ruoff, R. S. Graphene-Based Ultracapacitors. *Nano Lett.* **2008**, *8* (10), 3498–3502.

(65) Zhang, Y.; Tan, Y.-W.; Stormer, H. L.; Kim, P. Experimental Observation of the Quantum Hall Effect and Berry's Phase in Graphene. *Nature* **2005**, *438* (7065), 201–204.

(66) Novoselov, K. S.; Geim, A. K.; Morozov, S. V.; Jiang, D.; Katsnelson, M. I.; Grigorieva, I. V.; Dubonos, S. V.; Firsov, A. A. Two-Dimensional Gas of Massless Dirac Fermions in Graphene. *Nature* **2005**, *438* (7065), 197–200.

(67) Chunder, A.; Pal, T.; Khondaker, S. I.; Zhai, L. Reduced Graphene Oxide/Copper Phthalocyanine Composite and Its Optoelectrical Properties. *J. Phys. Chem. C* **2010**, *114* (35), 15129–15135.

(68) Mondal, P.; Sinha, A.; Salam, N.; Roy, A. S.; Jana, N. R.; Islam, S. M. Enhanced Catalytic Performance by Copper Nanoparticle–graphene Based Composite. *RSC Adv.* **2013**, *3* (16), 5615.

(69) Song, E. H.; Wen, Z.; Jiang, Q. CO Catalytic Oxidation on Copper-Embedded Graphene. *J. Phys. Chem. C* **2011**, *115* (9), 3678–3683.

(70) Jing, W.; Xiaochuan, G.; Yan, H.; Mingjun, J.; Weigui, Z. Synthesis and Tribological Properties of Graphene-Copper Nanoparticle Composites as Lithium Grease Additive. **2017**, *19* (4), 113–122.

(71) Wendorff, J. H.; Agarwal, S.; Greiner, A. *Electrospinning*; Wiley-VCH Verlag GmbH & Co. KGaA: Weinheim, Germany, 2012.

(72) Electrospinning Process. In *An Introduction to Electrospinning and Nanofibers*; World Scientific, 2005; pp 90–154.

(73) Yang, L.; Raza, A.; Si, Y.; Mao, X.; Shang, Y.; Ding, B.; Yu, J.; Al-Deyab, S. S. Synthesis of

Superhydrophobic Silica Nanofibrous Membranes with Robust Thermal Stability and Flexibility via in Situ Polymerization. *Nanoscale* **2012**, *4* (20), 6581.

(74) Li, D.; Xia, Y. Electrospinning of Nanofibers: Reinventing the Wheel? *Adv. Mater.* **2004**, *16* (14), 1151–1170.

(75) Shander, A. Introduction. *J. Cardiothorac. Vasc. Anesth.* **2013**, *27* (4), S1–S2.

(76) Zeng, J.; Xu, X.; Chen, X.; Liang, Q.; Bian, X.; Yang, L.; Jing, X. Biodegradable Electrospun Fibers for Drug Delivery. *J. Control. Release* **2003**, *92* (3), 227–231.

(77) Ding, B.; Wang, M.; Wang, X.; Yu, J.; Sun, G. Electrospun Nanomaterials for Ultrasensitive Sensors. *Mater. Today* **2010**, *13* (11), 16–27.

(78) Lin, J.; Tian, F.; Shang, Y.; Wang, F.; Ding, B.; Yu, J. Facile Control of Intra-Fiber Porosity and Inter-Fiber Voids in Electrospun Fibers for Selective Adsorption. *Nanoscale* **2012**, *4* (17), 5316.

(79) Babu, V. J.; Kumar, M. K.; Nair, A. S.; Kheng, T. L.; Allakhverdiev, S. I.; Ramakrishna, S. Visible Light Photocatalytic Water Splitting for Hydrogen Production from N-TiO_2 Rice Grain Shaped Electrospun Nanostructures. *Int. J. Hydrogen Energy* **2012**, *37* (10), 8897–8904.

(80) Lee, S. S.; Bai, H.; Liu, Z.; Sun, D. D. Electrospun TiO_2/SnO_2 Nanofibers with Innovative Structure and Chemical Properties for Highly Efficient Photocatalytic H_2 Generation. *Int. J. Hydrogen Energy* **2012**, *37* (14), 10575–10584.

(81) Bai, H.; Liu, Z.; Sun, D. D. The Design of a Hierarchical Photocatalyst Inspired by Natural Forest and Its Usage on Hydrogen Generation. *Int. J. Hydrogen Energy* **2012**, *37* (19), 13998–14008.

(82) Choi, S. K.; Kim, S.; Lim, S. K.; Park, H. Photocatalytic Comparison of TiO_2 Nanoparticles and Electrospun TiO_2 Nanofibers: Effects of Mesoporosity and Interparticle Charge Transfer. *J. Phys. Chem. C* **2010**, *114* (39), 16475–16480.

(83) Einert, M.; Weller, T.; Leichtweiß, T.; Smarsly, B. M.; Marschall, R. Electrospun CuO Nanofibers: Stable Nanostructures for Solar Water Splitting. *ChemPhotoChem* **2017**, *1* (7), 326–340.

(84) Nguyen, M. A.; Bedford, N. M.; Ren, Y.; Zahran, E. M.; Goodin, R. C.; Chagani, F. F.; Bachas, L.

G.; Knecht, M. R. Direct Synthetic Control over the Size, Composition, and Photocatalytic Activity of Octahedral Copper Oxide Materials: Correlation Between Surface Structure and Catalytic Functionality. *ACS Appl. Mater. Interfaces* **2015**, *7* (24), 13238–13250.

(85) Khan, K. . Stability of a Cu_2O Photoelectrode in an Electrochemical Cell and the Performances of the Photoelectrode Coated with Au and SiO Thin Films. *Appl. Energy* **2000**, *65* (1–4), 59–66.

(86) Hara, M.; Kondo, T.; Komoda, M.; Ikeda, S.; Kondo, J. N.; Domen, K.; Hara, M.; Shinohara, K.; Tanaka, A. Cu_2O as a Photocatalyst for Overall Water Splitting under Visible Light Irradiation. *Chem. Commun.* **1998**, No. 3, 357–358.

(87) Barreca, D.; Fornasiero, P.; Gasparotto, A.; Gombac, V.; Maccato, C.; Montini, T.; Tondello, E. The Potential of Supported Cu_2O and CuO Nanosystems in Photocatalytic H_2 Production. *ChemSusChem* **2009**, *2* (3), 230–233.

(88) Deng, X.; Wang, C.; Shao, M.; Xu, X.; Huang, J. Low-Temperature Solution Synthesis of CuO/Cu_2O Nanostructures for Enhanced Photocatalytic Activity with Added H_2O_2 : Synergistic Effect and Mechanism Insight. *RSC Adv.* **2017**, *7* (8), 4329–4338.

(89) Liu, M.; Qiu, X.; Miyauchi, M.; Hashimoto, K. Cu(II) Oxide Amorphous Nanoclusters Grafted Ti^{3+} Self-Doped TiO 2 : An Efficient Visible Light Photocatalyst. *Chem. Mater.* **2011**, No. Ii, 111108102439004–111108102439004.

(90) Xing, J.; Chen, Z. P.; Xiao, F. Y.; Ma, X. Y.; Wen, C. Z.; Li, Z.; Yang, H. G. $Cu\text{-}Cu_2O\text{-}TiO_2$ nanojunction Systems with an Unusual Electron-Hole Transportation Pathway and Enhanced Photocatalytic Properties. *Chem. - An Asian J.* **2013**, *8* (6), 1265–1270.

(91) Cho, D.; Choi, D.; Pawar, R. C.; Lee, S.; Yoon, E. H.; Lee, T. Y.; Lee, C. S. Simple Coating Method of Carbonaceous Film onto Copper Nanopowder Using PVP as Solid Carbon Source. *Mater. Chem. Phys.* **2014**, *148* (3), 859–867.

(92) Magdassi, S.; Grouchko, M.; Kamyshny, A. Copper Nanoparticles for Printed Electronics: Routes Towards Achieving Oxidation Stability. *Materials (Basel).* **2010**, *3* (9), 4626–4638.

(93) Engels, V.; Benaskar, F.; Jefferson, D. A.; Johnson, B. F. G.; Wheatley, A. E. H. Nanoparticulate Copper – Routes towards Oxidative Stability. *Dalt. Trans.* **2010**.

(94) Mattevi, C.; Kim, H.; Chhowalla, M. A Review of Chemical Vapour Deposition of Graphene on Copper. *J. Mater. Chem.* **2011**, *21* (10), 3324–3334.

(95) Kobayashi, Y.; Ishida, S.; Ihara, K.; Yasuda, Y.; Morita, T.; Yamada, S. Synthesis of Metallic Copper Nanoparticles Coated with Polypyrrole. *Colloid Polym. Sci.* **2009**, *287* (7), 877–880.

(96) Pulkkinen, P.; Shan, J.; Leppänen, K.; Känsäkoski, A.; Laiho, A.; Järn, M.; Tenhu, H. Poly(Ethylene Imine) and Tetraethylenepentamine as Protecting Agents for Metallic Copper Nanoparticles. *ACS Appl. Mater. Interfaces* **2009**, *1* (2), 519–525.

(97) Jeong, S.; Woo, K.; Kim, D.; Lim, S.; Kim, J. S.; Shin, H.; Xia, Y.; Moon, J. Controlling the Thickness of the Surface Oxide Layer on Cu Nanoparticles for the Fabrication of Conductive Structures by Ink-Jet Printing. *Adv. Funct. Mater.* **2008**, *18* (5), 679–686.

(98) Ng, K. H.; Penner, R. M. Electrodeposition of Silver–copper Bimetallic Particles Having Two Archetypes by Facilitated Nucleation. *J. Electroanal. Chem.* **2002**, *522* (1), 86–94.

(99) Cazayous, M.; Langlois, C.; Oikawa, T.; Ricolleau, C.; Sacuto, A. Cu-Ag Core-Shell Nanoparticles: A Direct Correlation between Micro-Raman and Electron Microscopy. *Phys. Rev. B* **2006**, *73* (11), 113402.

(100) Grouchko, M.; Kamyshny, A.; Ben-Ami, K.; Magdassi, S. Synthesis of Copper Nanoparticles Catalyzed by Pre-Formed Silver Nanoparticles. *J. Nanoparticle Res.* **2009**, *11* (3), 713–716.

(101) Grouchko, M.; Kamyshny, A.; Magdassi, S. Formation of Air-Stable Copper–silver Core–shell Nanoparticles for Inkjet Printing. *J. Mater. Chem.* **2009**, *19* (19), 3057.

(102) Prasai, D.; Tuberquia, J. C.; Harl, R. R.; Jennings, G. K.; Bolotin, K. I. Graphene: Corrosion-Inhibiting Coating. *ACS Nano* **2012**, *6* (2), 1102–1108.

(103) Du, X.; Skachko, I.; Barker, A.; Andrei, E. Y. Approaching Ballistic Transport in Suspended Graphene. *Nat. Nanotechnol.* **2008**, *3* (8), 491–495.

(104) Liu, L.; Ryu, S.; Tomasik, M. R.; Stolyarova, E.; Jung, N.; Hybertsen, M. S.; Steigerwald, M. L.; Brus, L. E.; Flynn, G. W. Graphene Oxidation: Thickness-Dependent Etching and Strong Chemical Doping. *Nano Lett.* **2008**, *8* (7), 1965–1970.

(105) Chen, S.; Brown, L.; Levendorf, M.; Cai, W.; Ju, S.-Y.; Edgeworth, J.; Li, X.; Magnuson, C. W.; Velamakanni, A.; Piner, R. D.; et al. Oxidation Resistance of Graphene-Coated Cu and Cu/Ni Alloy. *ACS Nano* **2011**, *5* (2), 1321–1327.

(106) Byun, S.-J.; Lim, H.; Shin, G.-Y.; Han, T.-H.; Oh, S. H.; Ahn, J.-H.; Choi, H. C.; Lee, T.-W. Graphenes Converted from Polymers. *J. Phys. Chem. Lett.* **2011**, *2* (5), 493–497.

(107) Sun, Z.; Yan, Z.; Yao, J.; Beitler, E.; Zhu, Y.; Tour, J. M. Growth of Graphene from Solid Carbon Sources. *Nature* **2010**, *468* (7323), 549–552.

(108) Lee, S.; Hong, J.; Koo, J. H.; Lee, H.; Lee, S.; Choi, T.; Jung, H.; Koo, B.; Park, J.; Kim, H.; et al. Synthesis of Few-Layered Graphene Nanoballs with Copper Cores Using Solid Carbon Source. *ACS Appl. Mater. Interfaces* **2013**, *5* (7), 2432–2437.

(109) Elayappan, V.; Panneerselvam, P.; Nemala, S.; Nallathambi, K. S.; Angaiah, S. Influence of PVP Template on the Formation of Porous TiO_2 Nanofibers by Electrospinning Technique for Dye-Sensitized Solar Cell. *Appl. Phys. A* **2015**, *120* (3), 1211–1218.

(110) Nuansing, W.; Ninmuang, S.; Jarernboon, W.; Maensiri, S.; Seraphin, S. Structural Characterization and Morphology of Electrospun TiO_2 nanofibers. *Mater. Sci. Eng. B Solid-State Mater. Adv. Technol.* **2006**, *131* (1–3), 147–155.

(111) Cheng, Y. H.; Subramaniam, V. P.; Gong, D.; Tang, Y.; Highfield, J.; Pehkonen, S. O.; Pichat, P.; Schreyer, M. K.; Chen, Z. Nitrogen-Sensitized Dual Phase Titanate/Titania for Visible-Light Driven Phenol Degradation. *J. Solid State Chem.* **2012**, *196*, 518–527.

(112) Ponhan, W.; Maensiri, S. Fabrication and Magnetic Properties of Electrospun Copper Ferrite ($CuFe_2O_4$) Nanofibers. *Solid State Sci.* **2009**, *11* (2), 479–484.

(113) Craig A. Grimes, G. K. M. *TiO_2 Nanotube Arrays: Synthesis, Properties, and Applications TiO_2*

Nanotube Arrays: Synthesis, Properties, and Applications; Springer, 2011.

(114) Samir, M.; Salama, M.; Allam, N. K. Sub-100 Nm TiO_2 Tubular Architectures for Efficient Solar Energy Conversion. *J. Mater. Chem. A* **2016**, *4* (24), 9375–9380.

(115) Zhang, Z.; Lee, J.; Yates, J. T.; Bechstein, R.; Lira, E.; Hansen, J. Ø.; Wendt, S.; Besenbacher, F. Unraveling the Diffusion of Bulk Ti Interstitials in Rutile TiO_2 (110) by Monitoring Their Reaction with O Adatoms. *J. Phys. Chem. C* **2010**, *114* (7), 3059–3062.

(116) Wang, M.; Wen, J.; Sawada, Y.; Hoshi, Y.; Hou, Z. Effect of Oxygen and WO_3 Additive on Anatase-to-Rutile Phase Transformation in TiO_2 Nanoparticles. *J. Therm. Anal. Calorim.* **2015**, *119* (1), 435–439.

(117) Naccache, C.; Meriaudeau, P.; Che, M.; Tench, A. J. Identification of Oxygen Species Adsorbed on Reduced Titanium Dioxide. *Trans. Faraday Soc.* **1971**, *67*, 506.

(118) Carter, E.; Carley, A. F.; Murphy, D. M. Evidence for O_2 - Radical Stabilization at Surface Oxygen Vacancies on Polycrystalline TiO_2. *J. Phys. Chem. C* **2007**, *111* (28), 10630–10638.

(119) Strunk, J.; Vining, W. C.; Bell, A. T. A Study of Oxygen Vacancy Formation and Annihilation in Submonolayer Coverages of TiO_2 Dispersed on MCM-48 †. *J. Phys. Chem. C* **2010**, *114* (40), 16937–16945.

(120) Choudhury, B.; Dey, M.; Choudhury, A. Defect Generation, d-d Transition, and Band Gap Reduction in Cu-Doped TiO_2 Nanoparticles. *Int. Nano Lett.* **2013**, *3* (1), 25.

(121) Baltazar, P.; Lara, V. H.; Córdoba, G.; Arroyo, R. Kinetics of the Amorphous - Anatase Phase Transformation in Copper Doped Titanium Oxide. *J. Sol-Gel Sci. Technol.* **2006**, *37* (2), 129–133.

(122) Li, L.; Shi, X.; M., C.; L., G. Atomic and Molecular Low-n Rydberg States in Near Critical Point Fluids. In *Advanced Aspects of Spectroscopy*; InTech, 2012.

(123) Slamet; Kusrini, E.; Afrozi, A. S.; Ibadurrohman, M. Photocatalytic Hydrogen Production from Glycerol-Water over Metal Loaded and Non-Metal Doped Titanium Oxide. *Int. J. Technol.* **2015**, *6* (4), 520–532.

(124) Jin, Z.; Zhang, X.; Li, Y.; Li, S.; Lu, G. 5.1% Apparent Quantum Efficiency for Stable Hydrogen Generation over Eosin-Sensitized CuO/TiO_2 photocatalyst under Visible Light Irradiation. *Catal. Commun.* **2007**, *8* (8), 1267–1273.

(125) Tao, J.; Sun, Z.; Cheng, Y.; Zhang, M.; Lv, J.; Shi, S.; He, G.; Jiang, X.; Chen, X.; Wang, X.; et al. Enhanced Photoelectrochemical Properties of Nanocrystalline TiO_2 Electrode by Surface Sensitization with Cu_xO Quantum Dots. *Sci. Rep.* **2017**, *7* (1).

(126) Mohamed, A. M.; Amer, A. W.; AlQaradawi, S. Y.; Allam, N. K. On the Nature of Defect States in Tungstate Nanoflake Arrays as Promising Photoanodes in Solar Fuel Cells. *Phys. Chem. Chem. Phys.* **2016**, *18* (32), 22217–22223.

(127) Wei, X.; Chen, M. Self-Decomposition Effect of Graphene Based CdSe Composites for Organic Dye in Dark. *J. Chil. Chem. Soc.* **2015**, *60* (3), 2988–2997.

(128) Tian, M.; Mahjouri-Samani, M.; Wang, K.; Puretzky, A. A.; Geohegan, D. B.; Tennyson, W. D.; Cross, N.; Rouleau, C. M.; Zawodzinski, T. A.; Duscher, G.; et al. Black Anatase Formation by Annealing of Amorphous Nanoparticles and the Role of the Ti_2O_3 Shell in Self-Organized Crystallization by Particle Attachment. *ACS Appl. Mater. Interfaces* **2017**, *9* (26), 22018–22025.

(129) Li, Y.; Hwang, D.-S.; Lee, N. H.; Kim, S.-J. Synthesis and Characterization of Carbon-Doped Titania as an Artificial Solar Light Sensitive Photocatalyst. *Chem. Phys. Lett.* **2005**, *404* (1–3), 25–29.

(130) Grabstanowicz, L. R.; Gao, S.; Li, T.; Rickard, R. M.; Rajh, T.; Liu, D. J.; Xu, T. Facile Oxidative Conversion of TiH_2 to High-Concentration Ti^{3+}-Self-Doped Rutile TiO_2 with Visible-Light Photoactivity. *Inorg. Chem.* **2013**, *52* (7), 3884–3890.

(131) Cheng, Y. H.; Subramaniam, V. P.; Gong, D.; Tang, Y.; Highfield, J.; Pehkonen, S. O.; Pichat, P.; Schreyer, M. K.; Chen, Z. Nitrogen-Sensitized Dual Phase Titanate/Titania for Visible-Light Driven Phenol Degradation. *J. Solid State Chem.* **2012**, *196*, 518–527.

(132) Pai, M. R.; Banerjee, A. M.; Rawool, S. A.; Singhal, A.; Nayak, C.; Ehrman, S. H.; Tripathi, A. K.;

Bharadwaj, S. R. A Comprehensive Study on Sunlight Driven Photocatalytic Hydrogen Generation Using Low Cost Nanocrystalline Cu-Ti Oxides. *Sol. Energy Mater. Sol. Cells* **2016**, *154*, 104–120.

(133) Leng, W.; Barnes, H. M.; Cai, Z.; Zhang, J. Temperature and Copper Concentration Effects on the Formation of Graphene-Encapsulated Copper Nanoparticles from Kraft Lignin. *Materials (Basel).* **2017**, *10* (6).

(134) Khan, A.; Rashid, A.; Younas, R.; Chong, R. A Chemical Reduction Approach to the Synthesis of Copper Nanoparticles. *Int. Nano Lett.* **2016**, *6* (1), 21–26.

(135) Dresselhaus, M. S.; Dresselhaus, G.; Saito, R.; Jorio, A. Raman Spectroscopy of Carbon Nanotubes. *Phys. Rep.* **2005**, *409* (2), 47–99.

(136) Reich, S.; Thomsen, C. Raman Spectroscopy of Graphite. *Philos. Trans. R. Soc. A Math. Phys. Eng. Sci.* **2004**, *362* (1824), 2271–2288.

(137) Thomsen, C.; Reich, S. Double Resonant Raman Scattering in Graphite. *Phys. Rev. Lett.* **2000**, *85* (24), 5214–5217.

(138) Ni, Z.; Wang, Y.; Yu, T.; Shen, Z. Raman Spectroscopy and Imaging of Graphene. *Nano Res.* **2008**, *1* (4), 273–291.

(139) Ding, J.; Yan, W.; Xie, W.; Sun, S.; Bao, J.; Gao, C. Highly Efficient Photocatalytic Hydrogen Evolution of Graphene/YInO3 Nanocomposites under Visible Light Irradiation. *Nanoscale* **2014**, *6* (4), 2299.

(140) Ahmed, N.; Farghali, A. A.; El Rouby, W. M. A.; Allam, N. K. Enhanced Photoelectrochemical Water Splitting Characteristics of TiO_2 hollow Porous Spheres by Embedding Graphene as an Electron Transfer Channel. *Int. J. Hydrogen Energy* **2017**, *42* (49), 29131–29139.

(141) Najafpour, M. M.; Rahimi, F.; Fathollahzadeh, M.; Haghighi, B.; Hołyńska, M.; Tomo, T.; Allakhverdiev, S. I. Nanostructured Manganese Oxide/Carbon Nanotubes, Graphene and Graphene Oxide as Water-Oxidizing Composites in Artificial Photosynthesis. *Dalt. Trans.* **2014**, *43* (28), 10866–10876.

(142) Dung, N. T.; Van Khoa, N.; Herrmann, J.-M. Photocatalytic Degradation of Reactive Dye RED-3BA in Aqueous TiO_2 Suspension under UV-Visible Light. *Int. J. Photoenergy* **2005**, *7* (1), 11–15.

(143) Zhang, X.; Wang, J.; Jia, H.; Yin, B.; Ding, L.; Xu, Z.; Ji, Q. Polyvinyl Pyrrolidone Modified Graphene Oxide for Improving the Mechanical, Thermal Conductivity and Solvent Resistance Properties of Natural Rubber. *RSC Adv.* **2016**, *6* (60), 54668–54678.

(144) Li, J.; Shen, B.; Hong, Z.; Lin, B.; Gao, B.; Chen, Y. A Facile Approach to Synthesize Novel Oxygen-Doped g-C3N4 with Superior Visible-Light Photoreactivity. *Chem. Commun.* **2012**, *48* (98), 12017.

(145) Murugan, A. V.; Muraliganth, T.; Manthiram, A. Rapid, Facile Microwave-Solvothermal Synthesis of Graphene Nanosheets and Their Polyaniline Nanocomposites for Energy Strorage. *Chem. Mater.* **2009**, *21* (21), 5004–5006.

(146) Dai, S.; Wu, Y.; Sakai, T.; Du, Z.; Sakai, H.; Abe, M. Preparation of Highly Crystalline TiO_2 Nanostructures by Acid-Assisted Hydrothermal Treatment of Hexagonal-Structured Nanocrystalline Titania/Cetyltrimethyammonium Bromide Nanoskeleton. *Nanoscale Res. Lett.* **2010**, *5* (11), 1829–1835.

(147) Cheng, G.; Hight Walker, A. R. Transmission Electron Microscopy Characterization of Colloidal Copper Nanoparticles and Their Chemical Reactivity. *Anal. Bioanal. Chem.* **2010**, *396* (3), 1057–1069.

(148) Zhang, S.; Peng, B.; Yang, S.; Wang, H.; Yu, H.; Fang, Y.; Peng, F. Non-Noble Metal Copper Nanoparticles-Decorated TiO_2 nanotube Arrays with Plasmon-Enhanced Photocatalytic Hydrogen Evolution under Visible Light. *Int. J. Hydrogen Energy* **2015**, *40* (1), 303–310.

VITA

Menna M. Hasan

Menna M. Hasan was born in Egypt on September 5, 1993. She graduated from Alexandria University, Alexandria, Egypt in 2015, with a bachelor's degree in chemistry/Environmental Science. Worked as a Research Assistant from Jan 2016 to May 2018 at The American University in Cairo, Cairo, Egypt. She has been awarded AlGhurair Foundation Fellowship to pursue MSc at The American University in Cairo. She has co-authored several publications on the fabrication of metal oxide nanofibers and their use in energy conversion applications such as photocatalytic water splitting.

Publications

1. Mohamed, M. A.; Hasan, M. M.; Abdullah, I. H.; Abdellah, A. M.; Yehia, A. M.; Ahmed, N.; Abbas, W.; Allam, N. K. Talanta Smart Bi-Metallic Perovskite Nano Fi Bers as Selective and Reusable Sensors of Nano-Level Concentrations of Non-Steroidal Anti-in Fl Ammatory Drugs. *Talanta* **2018**, *185* (February), 344–351
2. Menna M. Hasan, Nageh K. Allam. Unbiased Spontaneous Photocatalytic Water Splitting using Stable Erath Abundant Composite Nanofibers. Submitted.
3. Menna M. Hasan, Sarah A Tolba, Nageh K. Allam. In-situ Formation of Copper Nanoparticles Impeded in TiO_2 Nanofibers Significantly Enhances the Efficiency of Photocatalytic Water Splitting. Submitted.